

1 **Diatom–environment relationships and limnological variability: an**  
2 **updated quantitative tool for palaeoclimatology on sub-Antarctic**  
3 **Macquarie Island**

4 Caitlin A. Selfe<sup>1</sup>, Karina Meredith<sup>2</sup>, Liza McDonough<sup>2</sup>, Justine Shaw<sup>1</sup>, Stephen J. Roberts<sup>3</sup>, Krystyna M.  
5 Saunders<sup>4,5</sup>

6

7 <sup>1</sup> Securing Antarctica’s Environmental Future, Queensland University of Technology, Brisbane, 4000,  
8 Australia

9 <sup>2</sup> Securing Antarctica’s Environmental Future, Environment Research and Technology Group, Australian  
10 Nuclear Science and Technology Organisation, Lucas Heights, 2234, Australia

11 <sup>3</sup> British Antarctic Survey, Cambridge, CB3 0ET, United Kingdom

12 <sup>4</sup> Institute for Marine and Antarctic Studies, University of Tasmania, Hobart, 7004, Australia

13 <sup>5</sup> Australian Antarctic Division, Kingston, 7050, Australia

14

15 *Correspondence to:* Caitlin A. Selfe (caitlin.selfe@hrd.qut.edu.au)

16 **Keywords:** Diatoms, Electrical conductivity, sub-Antarctic, Macquarie Island, Transfer function, Southern

17 Hemisphere westerly winds, Palaeoclimate, Limnology

18 **Abstract.** Sub-Antarctic Macquarie Island is ideally located for reconstructing past variations in Southern  
19 Hemisphere westerly wind strength. Diatoms are a valuable palaeolimnological tool on sub-Antarctic  
20 islands, providing a means to reconstruct past climate and environmental changes. Diatom communities  
21 are sensitive to changes in lake electrical conductivity (EC) linked to westerly wind-driven sea-spray  
22 inputs on Macquarie Island, and diatom-conductivity models have previously been used to infer past  
23 westerly wind variability. Here we present new diatom data from 52 lakes to assess diatom-environment  
24 relationships and develop an updated diatom-conductivity model for Macquarie Island. Seasonal and  
25 multi-year water chemistry and isotope data were analysed to assess temporal variability in  
26 hydrochemical processes and the influence of evaporation, ensuring the resulting diatom-conductivity  
27 model reflects external climatic drivers rather than local dynamics. Statistically robust transfer functions  
28 were developed for EC (bootstrapped  $r^2 = 0.80$ , RMSEP = 0.40), while pH had weaker predictive  
29 performance. For EC, weighted averaging and maximum-likelihood approaches performed comparably,  
30 although the former showed reduced predictive power at high EC where low species turnover and  
31 nutrient collinearity affected accuracy. This quantitative-diatom model combined with understanding of  
32 hydrogeochemical processes provides an improved basis for reconstructing past Southern Hemisphere  
33 westerly wind variability, which can be applied in future palaeoclimate studies on Macquarie Island.

34

35

## 36 **1 Introduction**

37 The Southern Ocean region exerts a strong influence on Southern Hemisphere and global climates  
38 (Jones et al. 2016; Fogt and Marshall 2020). Sub-Antarctic islands are among the few landmasses  
39 located in the Southern Ocean, making them important sites for understanding the past and future role  
40 of the Southern Ocean on climate variability. The Southern Hemisphere westerly winds (SHW) are a  
41 major driver of Southern Hemisphere mid- to high-latitude climates, modulating ocean circulation, mid-  
42 latitude temperature and precipitation regimes, and the efficiency of the Southern Ocean carbon sink  
43 (Gillett et al. 2006; Le Quéré et al. 2009; Fletcher et al. 2021; Menviel et al. 2023; Thomas et al. 2025).  
44 Instrumental data show that in recent decades the SHW have intensified and shifted poleward in  
45 response to warming (Marshall 2003; Fogt and Marshall 2020). These changes have been linked to an  
46 increase in net outgassing of carbon dioxide (CO<sub>2</sub>) from deep-storage reservoirs in the Southern Ocean,  
47 with significant implications for future atmospheric CO<sub>2</sub> levels and global temperatures (Goyal et al. 2021;  
48 Nicholson et al. 2022; Mongwe et al. 2024; Olivier and Haumann 2025). Understanding long-term SHW  
49 variability is key to assessing the impacts of SHW dynamics under future climate warming scenarios.

50

51 Diatoms are highly sensitive to environmental changes and are widely used as palaeolimnological  
52 proxies to infer climate and environmental changes (Roberts et al. 2000; Verleyen et al. 2004; Sterken  
53 et al. 2008; Recasens et al. 2015; Liao et al. 2020; Peng et al. 2022; Deng et al. 2025). Diatoms are well  
54 established as indicators of salinity and ionic composition, forming the basis of numerous diatom–salinity  
55 or -conductivity transfer functions across a range of environments (Gasse et al. 1997; Verleyen et al.  
56 2003; Volik et al. 2017; Maslennikova 2020; Farqan et al. 2025). These approaches have been  
57 successfully applied in diverse settings demonstrating the reliability of diatom assemblages for  
58 reconstructing past hydrochemical and environmental change.

59

60 Previous work on sub-Antarctic Islands has demonstrated that aquatic diatom communities are  
61 significantly influenced by changes in salinity (inferred from electrical conductivity [EC]), allowing  
62 quantitative diatom-conductivity models to be developed (Gremmen et al. 2007; Saunders et al. 2009;  
63 2015; 2018; Perren et al. 2020; Van Nieuwenhuyze 2020; Perren et al. 2025). On sub-Antarctic islands,  
64 lake water salinity changes are largely controlled by wind-driven sea spray aerosol (SSA) inputs, via both  
65 wet and dry deposition, with increased inputs occurring when winds are stronger and vice versa (Evans

66 1970; Buckney and Tyler 1974; Saunders et al. 2009; 2015; Humphries et al. 2021). Based on this,  
67 diatom-conductivity transfer functions have been used to infer past Holocene SHW intensity on  
68 Macquarie Island (Saunders et al., 2018), Marion Island (Perren et al. 2020) and in southern South  
69 America (Perren et al. 2025). These relationships are understood to reflect longer-term, integrated  
70 hydrogeochemical and ecological responses to persistent wind-driven sea-spray inputs, rather than  
71 event-scale meteorological forcing.

72

73 Earlier studies on Macquarie Island have analysed diatom-environment relationships (McBride 2009;  
74 Saunders et al. 2009) and their application as palaeoenvironmental and climate proxies (Keenan 1995;  
75 Saunders et al. 2013; 2018; Deng et al. 2025). However, from the late 1900s to early 2000s overgrazing  
76 from increasing invasive rabbit populations (up to 150,000 individuals estimated from 2005-2006)  
77 resulted in widespread ecosystem degradation, including erosion, vegetation loss, and altered organic  
78 inputs into lakes (Scott and Kirkpatrick 2008; Terauds 2009). This affected aquatic ecosystems and  
79 diatom diversity (Marchant et al. 2011; Saunders et al. 2013). The Macquarie Island Pest Eradication  
80 Programme successfully eradicated all invasive vertebrates (principally rabbits) from the island in 2011,  
81 triggering substantial ecosystem recovery (Springer, 2018; Fitzgerald et al., 2021). Although direct  
82 limnological data to assess ecosystem recovery of individual lakes is not available, widespread  
83 vegetation recovery following early efforts of the eradication programme in 2010-2011 provides strong  
84 evidence that ecosystem processes across the island are no longer characterised by extreme  
85 disturbance (Shaw et al. 2011; Springer 2018; Fitzgerald et al. 2021). This is expected to have decreased  
86 catchment erosion and sediment and nutrient delivery into lakes relative to the peak disturbance period,  
87 resulting in post-eradication (recovering) ecosystems.

88

89 Reassessing diatom–environment relationships under current post-eradication conditions is necessary,  
90 because earlier studies were conducted during a period of vertebrate-induced disturbance rather than  
91 under near-natural conditions (Saunders et al., 2013). Developing new diatom models based on post-  
92 eradication conditions may better represent pre-invasion baseline communities, improving the accuracy  
93 and ecological relevance of palaeolimnological reconstructions. Furthermore, incorporating revised  
94 taxonomy and newly identified species will enhance the model’s ecological resolution and predictive  
95 performance.

96

97 Understanding the processes that drive lake water chemistry, such as precipitation, evaporation,  
98 groundwater inputs, and nutrient cycling, and how they vary across temporal and spatial scales is  
99 essential when interpreting diatom–environmental relationships. Meredith et al. (2022) defined lake  
100 hydrogeochemical processes across Macquarie Island showing that dominant processes vary locally,  
101 and lakes can be classified as predominantly influenced by SSAs, catchment processes (i.e., with greater  
102 water-rock interaction), or precipitation (i.e., more dilute lake waters). Sea-spray-influenced lakes occur  
103 near the west coast and on the western edge on the Macquarie Island plateau, where exposure to the  
104 SHW is greatest. In contrast, catchment-influenced lakes with higher terrestrial ion concentrations are  
105 found at lower elevations, and rainfall-influenced lakes with low ion concentrations occur at higher  
106 elevations. This hydrogeochemical framework supports the hypothesis that for lakes near the west coast,  
107 including those on the western edge of the plateau, EC-related diatom variation on Macquarie Island  
108 primarily reflects SHW-driven sea-spray inputs rather than local hydrological or geochemical controls.

109

110 While present day water chemistry provides valuable insight into spatial variability, it is necessary to  
111 quantify temporal variability in hydrogeochemical processes, particularly evaporation, to assess how  
112 seasonal, interannual, and longer-term changes modify ion concentrations in lakes, including those  
113 derived from SSA. Establishing seasonal and multi-year lake water hydrogeochemical datasets will  
114 enhance confidence in proxy interpretations and form a foundation for long-term monitoring of Macquarie  
115 Island lakes. Such research is rarely applied to develop ecological transfer functions particularly in such  
116 remote, isolated settings, and has not yet been undertaken on other sub-Antarctic islands. These factors  
117 highlight the importance of this work for understanding how sub-Antarctic Island ecosystems will respond  
118 to future climate and environmental changes, particularly given the rapid ecological shifts in response to  
119 climate that are already documented across the region (le Roux and McGeoch 2008; Lee and Chown  
120 2016; Nel et al. 2023).

121

122 Here, we present new data from lakes on Macquarie Island quantifying post-pest eradication  
123 relationships between surface-sediment diatom communities and environmental conditions. Using  
124 comprehensive water chemistry datasets from 2018 and 2022–23, we examine seasonal and interannual  
125 variability to develop updated diatom–environment transfer functions. This integrated approach  
126 strengthens the application of diatom-based proxies and provides a first step towards long-term  
127 monitoring of sub-Antarctic lake systems by contributing to baseline data and establishing an analytical

128 framework to track ecological and biogeochemical change. These transfer functions will be applied in  
129 future studies to reconstruct past Holocene climate variability on Macquarie Island.

## 130 **2 Methods and Materials**

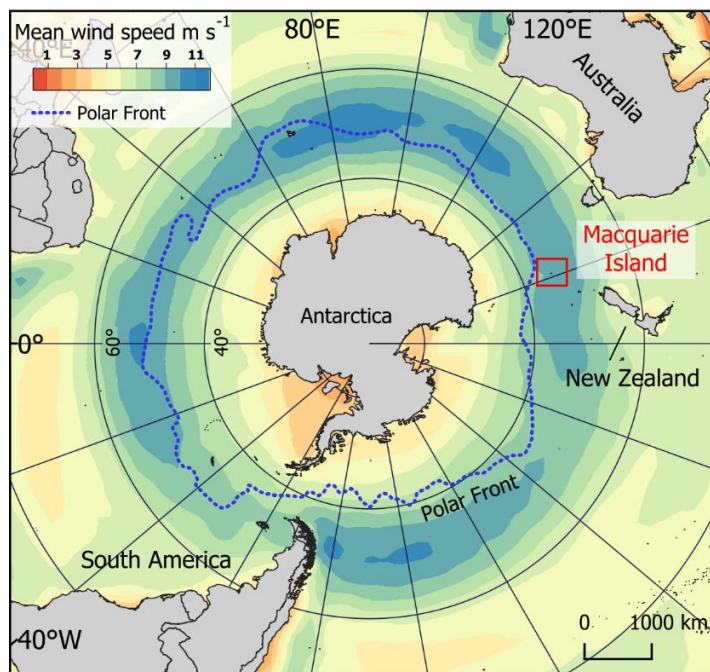
### 131 **2.1 Study area: Macquarie Island**

132 Macquarie Island (54°50'S, 158°85'E) is a small sub-Antarctic island (128 km<sup>2</sup>) located in the Southern  
133 Ocean just north of the polar front, 1,200 km south-west of New Zealand and 1,300 km from the Antarctic  
134 continent (Fig. 1). It is one of the few landmasses within the Polar Frontal Zone and modern core SHW  
135 belt (50–55°S; Fig.1), making it ideally suited to study past and current changes in the SHW, temperature,  
136 and precipitation. It has a harsh, cool, wet, oceanic climate with low seasonality and high wind velocities  
137 throughout the year. Together, these represent the influence the SHW have on climate in the region  
138 (Selkirk et al. 1990). The SHW prevail almost exclusively from the west and north-west with a mean  
139 annual wind speed of 35 km h<sup>-1</sup> and gusts reaching 185 km h<sup>-1</sup> (between 1948-2025; BOM 2025). The  
140 continual dominance of the SHW drive environmental and ecosystems responses on a west-to-east  
141 gradient across the island (Chau et al. 2019; Meredith et al. 2022), including the deposition and  
142 accumulation of wind-blown inputs such as sea spray and minerogenic aerosols (Buckney and Tyler  
143 1974; Saunders et al. 2009). Mean annual temperature ranges from 3.1–6.6°C, and the island  
144 experiences high annual rainfall of >1000 mm with >317 rainy days yr<sup>-1</sup> (between 1948–2025; BOM  
145 2025). Rainfall has increased in recent decades with a higher frequency of intense rainfall events, mostly  
146 occurring during winter, which are then accompanied by drier, windier summers (Andersen et al. 2009;  
147 Kong et al. 2025). Persistent cloud cover over the island results in low light levels and sunshine hours  
148 per day (average 2.4 h from 1948–2022; BOM, 2025).

149

150 Macquarie Island is geologically unique, being the only location worldwide where an intact marine  
151 ophiolite sequence of oceanic crust and upper mantle is exposed above sea level (Davis, 1987). The  
152 island is composed mostly of pillow basalts with interspersed flows of massive basalt (Selkirk et al. 1990).  
153 Dolerite, ultrabasics and intrusives are also present but are confined to the northern third of the island  
154 (Mawson 1943). As widespread glaciation did not occur during the Last Glacial Maximum (26–20 ka),  
155 marine, periglacial and subaerial erosional, rather than glacial processes, shaped the island as well as  
156 lake formation and ontogeny. The island is fringed by a low coastal terrace leading to steep-sided slopes

157 (20–40°) that rise to form the island plateau sitting at ~200–400 m asl (Selkirk et al. 1990; McBride and  
158 Selkirk 1998).



159  
160 Fig 1: Location of Macquarie Island in the Southern Ocean and mean annual wind speeds around the Southern Hemisphere  
161 (ERA5 reanalysis data 1960-2025), showing that the island lies within the modern core Southern Hemisphere westerly wind  
162 belt (50–55°S).

163 The island has numerous shallow and deep lakes and ponds across the plateau and coastal terrace (Fig.  
164 2). High accumulation of surface water and a high water-table at or very near the surface lead to the  
165 formation of extensive mires across the island (Löffler 1984). While lake edges can form thick ice cover  
166 during winter, complete freezing of the lakes is not typically observed (Evans 1970; Selkirk-Bell and  
167 Selkirk 2013). The island is vegetated by bryophytes, tussock grass, herbs and sedges, with no shrub  
168 or tree species present (Selkirk et al. 1990).

## 169 2.2 Data collection

170 Surface sediments and water samples were collected from lakes on Macquarie Island during the 2022–  
171 23 austral summer (referred to as 2022). Sites were selected to replicate those sampled in 2018 that  
172 were published by Meredith et al. (2022).

173 Lake surface sediments were collected from 30 plateau (inland) sites for diatom analyses (lake ID = LK),  
174 representing conditions more than 10 years post-rabbit and rodent eradication. Surface sediments (top  
175 2 cm) were collected from each site using a long-handled scoop from <1.5 m water depth. This method  
176 for sediment collection was selected for its logistical feasibility. Sediment mixing was minimised by  
177 visually assessing sampling depth and subsampling where necessary to retain only the upper ~2 cm.  
178 Sediments were generally well consolidated and remained intact during collection. Based on available  
179 lead-210 ( $^{210}\text{Pb}$ ) chronologies from Macquarie Island lake cores, this interval represents approximately  
180 10 years of accumulation (Saunders et al. 2013; Saunders et al. 2018), comparable to surface sediment  
181 sampling approaches used in previous studies (e.g. Saunders et al., 2009). An additional 17 coastal and  
182 five plateau sites sampled in 2006 (lake ID = S; Saunders et al. 2009) were included in the diatom dataset  
183 to extend the EC and nutrient gradients of the updated dataset, totalling 52 samples (Fig. 2a). Two lakes  
184 were replicated in the 2006 and 2022 seasons (S9 = LK40, S18 = LK2; Fig. 2a).

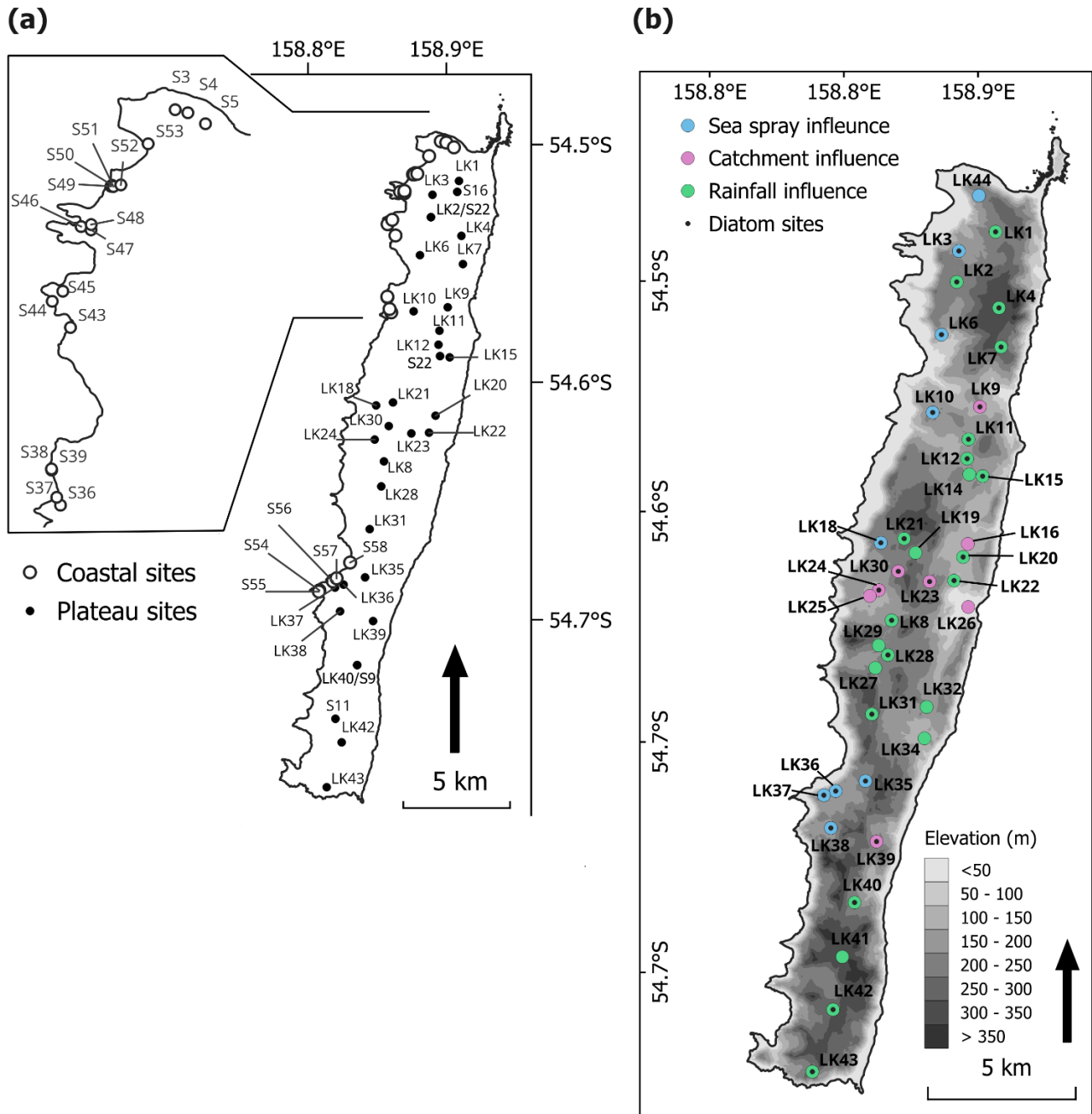
185

186 Lake water general parameters were measured in-situ at each site, including temperature, EC, dissolved  
187 oxygen (DO), and pH using a YSI ProQuatro Multiparameter Meter, with calibration performed prior to  
188 every sampling trip. DO was calibrated in water-saturated air following YSI manufacturer protocols.  
189 Conductivity was calibrated using a  $1413 \mu\text{S cm}^{-1}$  standard solution, and pH was calibrated using a  
190 three-point procedure with pH 4.0, 7.0, and 10.0 buffer solutions. Water samples were collected at all  
191 diatom sampling sites to measure total oxidised nitrogen (TON), phosphate ( $\text{PO}_4^{3-}$ ), and silica (Si).  
192 Additional water samples were collected from 40 plateau sites for water chemistry analysis (Fig. 2b),  
193 including major ions and stable water isotopes (oxygen [ $\delta^{18}\text{O}$ ] and hydrogen [ $\delta^2\text{H}$ ]). Each site was  
194 sampled three times across the 2022–23 season (November, December to January, and February). All  
195 water samples were collected from ~20 cm below the water surface and were filtered in-situ with  $0.45$   
196  $\mu\text{m}$  polyethersulphone filters into High Density Poly-Ethylene (HDPE) bottles following the method  
197 described by Meredith et al. (2009)). Water samples were refrigerated ( $4^\circ\text{C}$ ) until analysis.

198

199 Major ions, and oxygen ( $\delta^{18}\text{O}$ ) and hydrogen ( $\delta^2\text{H}$ ) stable isotopes were analysed at the Australian  
200 Nuclear Science and Technology Organisation (ANSTO). Cations and anions were analysed using  
201 inductively coupled plasma-atomic emission spectrometry (ICP-AES).  $\delta^{18}\text{O}$  and  $\delta^2\text{H}$  stable isotopes were  
202 analysed with a Picarro L2130-i Cavity Ring-Down Spectrometer. Values were reported as per mill (‰)

203 deviations relative to the international standard V-SMOW (Vienna Standard Mean Ocean Water), with a  
204 reproducible precision of  $\pm 0.2$  and  $\pm 1.0\text{‰}$ , respectively.



205 Fig. 2: Maps showing lake sites across Macquarie Island, **a**) Diatom surface sediment sites (coastal sites were originally sampled  
206 by Saunders et al. (2009); **b**) Lake water chemistry sites. Colours show lake types, based on dominate hydrogeochemical  
207 processes, identified by Meredith et al., (2022). Black dots indicate that the site is also included in the diatom dataset.

208 Nutrient data from 2006 samples (filtered at 0.45 $\mu$ m) measured soluble reactive phosphate (SRP), TON  
209 (nitrate [NO<sub>3</sub>] + nitrite [NO<sub>2</sub>]), and silicate (Si) using an Alpkem Autoanalyser (Continuous Flow Solution  
210 Analyser), representing the operationally defined dissolved inorganic (and therefore readily bioavailable)  
211 fractions of total N, P, and Si. In contrast, the 2022 dataset measured TON, PO<sub>4</sub><sup>3-</sup>, and Si ions using  
212 ICP-AES at ANSTO on filtered, undigested waters, with results reported as the corresponding inorganic  
213 species and concentrations consistently at or near detection limits. Despite methodological differences,  
214 the two approaches yield consistently low and broadly comparable concentrations in the two replicate  
215 lakes across sampling trips: for S9/LK40, PO<sub>4</sub><sup>3-</sup> concentrations were 0.002 mg L<sup>-1</sup> (autoanalyser) and  
216 <0.01 mg L<sup>-1</sup> (ICP-AES), and TON concentrations were 0.006 mg L<sup>-1</sup> (autoanalyser) and <0.06 mg L<sup>-1</sup>  
217 (ICP-AES); for S18/LK2, PO<sub>4</sub><sup>3-</sup> concentrations were 0.004 mg L<sup>-1</sup> (autoanalyser) and <0.01 mg L<sup>-1</sup> (ICP-  
218 AES), and TON concentrations were 0.005 mg L<sup>-1</sup> (autoanalyser) and <0.06 mg L<sup>-1</sup> (ICP-AES).  
219 Furthermore, if the 2022 analyses targeted the same reactive fractions measured in 2006, the results  
220 would still fall below or close to detection limits.

## 221 **2.3 Diatom preparation and identification**

222 Diatom preparation followed methods described by McBride (2009). Cleaned diatom solutions were  
223 mounted onto slides using Norland Optical Adhesive 61. At least 300–400 frustules were counted per  
224 sample, using Differential Interference Contrast (DIC) and oil immersion at 1000x magnification on a  
225 Zeiss Axioskope microscope, mounted with a TOUPTEK camera (U3CMOS). Species identification was  
226 primarily based on sub-Antarctic taxonomy described in Van de Vijer et al. (2002); Sterken et al. (2015);  
227 Sabbe et al. (2019); and Van de Vijver (2019). Species were photographed and documented (see  
228 Supplementary Material for an illustrated species catalogue).

## 229 **2.4 Statistical analyses**

### 230 **2.4.1 Water chemistry**

231 The lake water chemistry dataset was comprised of *in-situ* general parameters, major ion concentrations  
232 and  $\delta^{18}\text{O}$  and  $\delta^2\text{H}$  values from 2018 (Meredith et al. 2022) and 2022 (this study) to understand temporal  
233 variation across the island. Data from 2018 (January to February) are referred to as sampling event 1  
234 (E1) and sampling from the 2022 season as E2 (November), E3 (December to January), and E4  
235 (February). Shapiro–Wilk tests showed that isotope data were normally distributed ( $p > 0.05$ ), whereas

236 general parameters and ion concentrations deviated significantly from normality ( $p < 0.05$ ).  
237 Consequently, parametric tests (ANOVA, t-test, Tukey's HSD) were applied to normally distributed  
238 isotope data, and non-parametric tests (Kruskal–Wallis, pairwise Wilcoxon) to non-normally distributed  
239 general parameters ion data. Principal Component Analysis (PCA) with z-score standardised data was  
240 performed to explore relationships between variables and assess the consistency of lake types identified  
241 by Meredith et al. (2022; Fig. 2b).

#### 242 **2.4.2 Diatom model**

243 Diatom inference models were developed using diatom and environmental data collected from 2006 and  
244 2022. Ordination methods were used to describe variation in the diatom dataset, explore diatom-  
245 environment relationships, and identify unique variance explained by environmental variables.  
246 Environmental variables included were EC, temperature, DO, pH, TON,  $\text{PO}_4^{3-}$ , and Si, with mean 2022  
247 values used. Additional major ions were not included as these data were not available for 2006 sites.  
248 Water depth was not included as a variable as all sediment samples were collected within a narrow range  
249 of 0–1.5 m water depth, rendering ecological changes in depth negligible. Additionally, water depth is  
250 often regarded as a composite variable that acts as a surrogate for complex environmental gradients  
251 (e.g., habitat type, light, salinity, nutrients, oxygen, and taphonomy) that are largely unknown and  
252 unquantified, and therefore its inclusion can lead to spurious and misleading results (Birks et al. 1998;  
253 Juggins 2013). Weighted Averaging (WA) was applied to determine species ecological optima and  
254 tolerance. Together WA, Weighted Averaging Partial Least Squares (WAPLS), and Maximum Likelihood  
255 (ML) models were used to develop diatom transfer functions, with cross-validation used to assess model  
256 robustness.

257

258 The relative abundance of each diatom species in each sample was calculated as the percentage of the  
259 total number of frustules counted per sample. Species occurring at  $\leq 1\%$  relative abundance were  
260 excluded from the dataset. A full species list can be found in Supplementary Material. Nutrient values  
261 that were below the limit of detection were substituted with the respective detection limit value ( $\text{PO}_4^{3-}$ , =  
262  $0.01 \text{ mg L}^{-1}$ , Si =  $0.1 \text{ mg L}^{-1}$ , TON =  $0.06 \text{ mg L}^{-1}$ ). Environmental variables were screened for skewness,  
263 with temperature, EC,  $\text{PO}_4^{3-}$ , Si, and TON  $\log(x+1)$  transformed.

264

265 PCA was performed on transformed environmental data to identify the primary gradients of  
266 environmental variation across sites. Detrended Correspondence Analysis (DCA) with detrending by  
267 segments and downweighting of rare species was performed on untransformed species data to  
268 determine whether species distributions were linear or unimodal. As the DCA axis 1 gradient length (8.2  
269 deviation units) was  $> 4$ , unimodal ordination methods were deemed appropriate (Ter Braak and Prentice  
270 1988). Species data were  $\log(x+1)$  transformed for remaining analysis.

271

272 A series of Canonical Correspondence Analyses (CCA) were then performed with forward selection, and  
273 scaling focused on inter-species distances, biplot scaling and downweighting of rare species. Variance  
274 Inflation Factors (VIF) of environmental variables were used to assess collinearity. As no variables had  
275 a VIF  $> 10$ , none were excluded. A full CCA, with all environmental variables included, was first performed  
276 to quantify the total amount of species–environment variance explained by the full set of variables. A  
277 series of independent and partial CCAs with variance partitioning were performed to constrain analyses,  
278 assess the relative explanatory power, and assess the unique and shared variance contributions of each  
279 variable. Individual CCAs, of each variable alone, estimate the marginal (unconstrained) explanatory  
280 power (i.e., how much variation a single variable explains when considered alone, without accounting  
281 for correlations with other variables). Partial CCAs assess the unique (conditional) contribution of each  
282 environmental variable after statistically controlling for all remaining variables. This analysis isolates the  
283 variance uniquely attributable to each predictor and identifies variables whose explanatory power is  
284 driven by covariation with others. Finally, variance partitioning was used to decompose the total  
285 explained variation into unique and shared fractions, allowing assessment of how much variation was  
286 due to individual predictors versus overlapping environmental gradients. Permutation test results ( $p >$   
287  $0.05$ ), CCA coefficients and lambda ratios ( $\lambda_1/\lambda_2$ ) of the first constrained eigenvalue ( $\lambda_1$ ) to the second  
288 unconstrained eigenvalue ( $\lambda_2$ ) were used to identify the environmental variables most appropriate for  
289 quantitative inference models. As a guide, high  $\lambda_1/\lambda_2$  ratios are necessary for a variable to have enough  
290 explanatory power to be included in quantitative inference models (Ter Braak and Prentice 1988; Juggins  
291 2013). All ordination analyses were performed using the *vegan* package version 2.7-1 (Oksanen et al.  
292 2013) in R (R Core Team, 2024).

293

294 ML and iterations of inverse ( $_{INV}$ ) and classical ( $_{CLA}$ ) WA models with and without tolerance downweighting,  
295 and WAPLS with up to five components were assessed to determine the best performing transfer

296 functions. These methods were applied because they capture different aspects of species–environment  
297 relationships: WA provides a simple unimodal estimator; WAPLS allows more complex responses  
298 through latent components; and ML emphasises taxa with narrow ecological tolerances. Using multiple  
299 approaches therefore offers complementary strengths and helps identify the most reliable and robust  
300 model through cross-validation. All models were performed with bootstrapping and 100 iterations. Model  
301  $R^2$ , bootstrapped  $R^2$  ( $R_{boot}^2$ ), root mean square error (RMSE) and root mean square error of prediction  
302 (RMSEP) values were used to assess performance. RMSEP and  $R_{boot}^2$  performance was favoured over  
303  $R^2$  and RMSE. RMSEP between WAPLS components was also used to assess overfitting. WA and  
304 WAPLS-1 results are often similar as WAPLS is built upon on the same weighted-averaging framework  
305 as WA (ter Braak and Juggins 1993). When this was the case and WAPLS components did not improve  
306 performance, WA was favoured as the most parsimonious model. Software program C2 version 1.8  
307 (Juggins 2003) was used to develop all transfer functions.

## 308 **3 Results**

### 309 **3.1 Lake water chemistry**

310 Analyses of 40 plateau lakes on Macquarie Island showed that lake water general parameters (EC, pH  
311 and DO), and nutrients, did not vary significantly ( $p > 0.01$ ) across the 2022 sampling events (E2-4; Table  
312 1). Temperature varied, being significantly lower in E2 compared to E3 and E4 ( $p < 0.01$ ). Lakes were  
313 moderately acidic (pH 5.7) to alkaline (pH 9.14). Mean EC ranged from 126–261  $\mu\text{S cm}^{-1}$ , with a decrease  
314 in EC from west to east across the island. Lakes were oxic (DO = 8.64–12.61  $\text{mg L}^{-1}$ ) and oligotrophic,  
315 with  $\text{PO}_4^{3-}$  and TON concentrations under or close to detection limits ( $< 0.01$ – $0.02 \text{ mg L}^{-1}$  and  $< 0.06$ – $0.1$   
316  $\text{mg L}^{-1}$ , respectively). Similarly, comparison with data from plateau lakes sampled in 2018 showed no  
317 significant difference ( $p > 0.01$ ) across all lake water general parameters, excluding temperature,  
318 indicating generally stable conditions in plateau lakes across years. However, a comparison between  
319 plateau lakes measured in 2022 and coastal lakes in 2006 did show significant differences ( $p < 0.01$ ).  
320 Coastal sites in 2006 were generally eutrophic with higher nutrient ranges (TON = 0.007–4.636  $\text{mg L}^{-1}$   
321 and  $\text{PO}_4^{3-} = 0.1$ – $9.9 \text{ mg L}^{-1}$ ), and higher EC (406–1482  $\mu\text{S cm}^{-1}$ ), while temperature, DO, pH, Si were  
322 not significantly different ( $p > 0.01$ ) (Table 1; see Table S1 and S2 for full results).

323

324

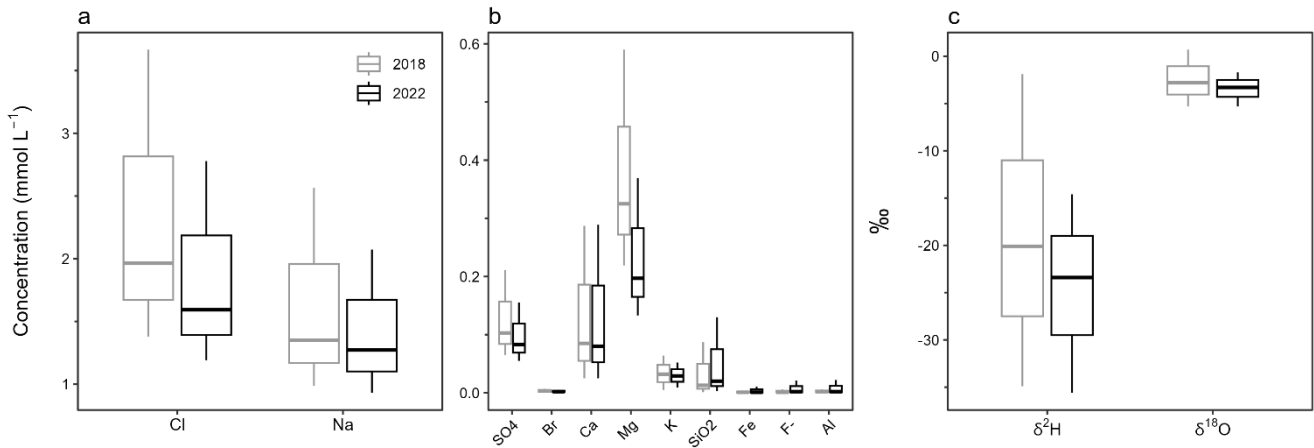
325 Table 1: Summary of lake water general parameters and nutrient data. Temp. = temperature, DO = dissolved oxygen, EC =  
 326 electrical conductivity, Si = silicate, PO<sub>4</sub><sup>3-</sup> = phosphate, TON = total oxidised nitrogen.

	Temp. (°C)	DO (mg L <sup>-1</sup> )	EC (µs cm <sup>-1</sup> )	pH	Si (mg L <sup>-1</sup> )	TON (mg L <sup>-1</sup> )	PO <sub>4</sub> <sup>3-</sup> (mg L <sup>-1</sup> )
<b>2022</b>							
Mean	8.7	11.59	188	7.03	0.648	0.06	0.00467
Min	6.4	8.69	135	5.65	0.100	0.06	0.00326
Max	16.1	12.95	267	9.15	4.333	0.10	0.02391
E1 mean (n=39)	7.6	12.47	188	7.02	0.767	0.06	0.00568
E2 mean (n=37)	9.1	11.94	197	7.03	0.611	0.06	0.00414
E3 mean (n=39)	9.6	10.48	177	7.05	0.515	0.06	0.00351
<b>2018 (n=40)</b>							
Mean	9.4	10.95	153	7.35	-	-	-
Min	6.8	8.56	101	5.99	-	-	-
Max	15.8	12.64	292	9.21	-	-	-
<b>2006 (plateau) (n=5)</b>							
Mean	6.4	11.59	192	6.92	0.047	0.00564	0.0070
Min	5.5	11.35	164	6.35	0.003	0.00004	0.0013
Max	7.4	11.80	224	7.46	0.092	0.02449	0.0155
<b>2006 (coastal) (n=17)</b>							
Mean	8.4	11.32	889	7.19	0.719	1.23331	1.124
Min	6.0	9.17	406	5.50	0.074	0.02430	0.007
Max	13.1	14.43	1482	8.13	2.706	9.89000	4.636

327  
 328 Major ion analysis of the 40 plateau lakes showed that, although dilute in concentration, Cl (1.1–3.7  
 329 mmol L<sup>-1</sup>) and Na (0.9–2.6 mmol L<sup>-1</sup>) dominate the ionic composition of all lake waters (Fig. 3; see  
 330 Supplementary Table S3 for full cation and anion results). All lakes showed similar ionic ratios to  
 331 seawater for SO<sub>4</sub>, Cl, Mg, and Na, suggesting a marine origin. Seawater ionic ratios diverged for K, Ca  
 332 and F for some lakes, while SiO<sub>2</sub> was higher in all lakes, suggesting additional sources for these ions.  
 333 (Fig. 4).

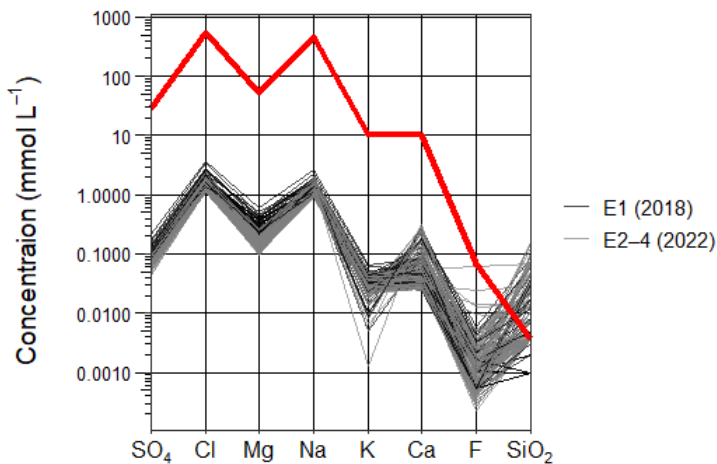
334  
 335 Statistical analyses showed no significant ( $p > 0.005$ ) differences in major ion concentrations across 2022  
 336 sampling events (E2–4). Broader changes were detected between 2018 and 2022, with Cl, SO<sub>4</sub>, Br, and  
 337 Mg all showing significantly higher mean concentrations ( $p < 0.005$ ) in 2018 compared to all 2022

338 sampling events (E2–4). Fe, Na, K, Ca, F, SiO<sub>2</sub>, and Al did not significantly vary ( $p > 0.005$ ) between  
339 sampling events. All ions that show significant variation ( $p < 0.005$ ) have predominantly marine sources.



340

341 Fig. 3: Box and whisker plots showing the range and mean of 2018 and 2022 lake water major ions **a)** Cl and Na; **b)** SO<sub>4</sub>, Br,  
342 Ca, Mg, K, SiO<sub>2</sub>, Fe, F<sup>-</sup>, and Al; and **c)** stable water isotopes δ<sup>2</sup>H and δ<sup>18</sup>O.

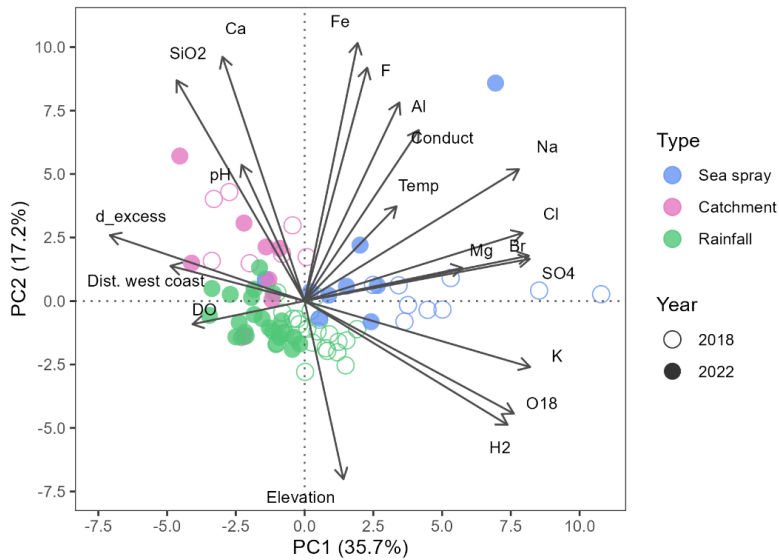


343

344 Fig. 4: Scholler plot comparing the ionic composition (SO<sub>4</sub>, Cl, Mg, Na, K, Ca, F and SiO<sub>2</sub>) of Macquarie Island lake waters and  
345 seawater (red line), categorised into sampling years 2018 (black lines) and 2022 (grey lines).

346 A PCA shows the relationship between lake water chemistry parameters, with samples grouped by lake  
347 type and sampling year (Fig. 5). Together, PC1 and PC2 captured 53% of the total variance in the  
348 dataset. PC1 represents a salinity and sea-spray gradient with variability in EC, distance from the west  
349 coast, Na, Cl, Br, Ca, Mg, and K captured. PC2 represents an altitude and terrestrial ion gradient with

350 variability in elevation, temperature, SiO<sub>2</sub>, Ca, Fe, and F captured. Lakes cluster according to  
 351 environmental processes (groups derived from Meredith et al., 2022), with SSA influenced lakes having  
 352 positive PC1 scores, which suggests higher concentrations of marine derived ions. The grouping of  
 353 samples influenced by catchment processes and those influenced by rainfall is driven by PC2 with  
 354 catchment influenced lakes having lower elevation and higher ion concentrations. SSA and rainfall  
 355 influenced lakes cluster based on the year that they were sampled with greater ion concentrations in  
 356 2018.

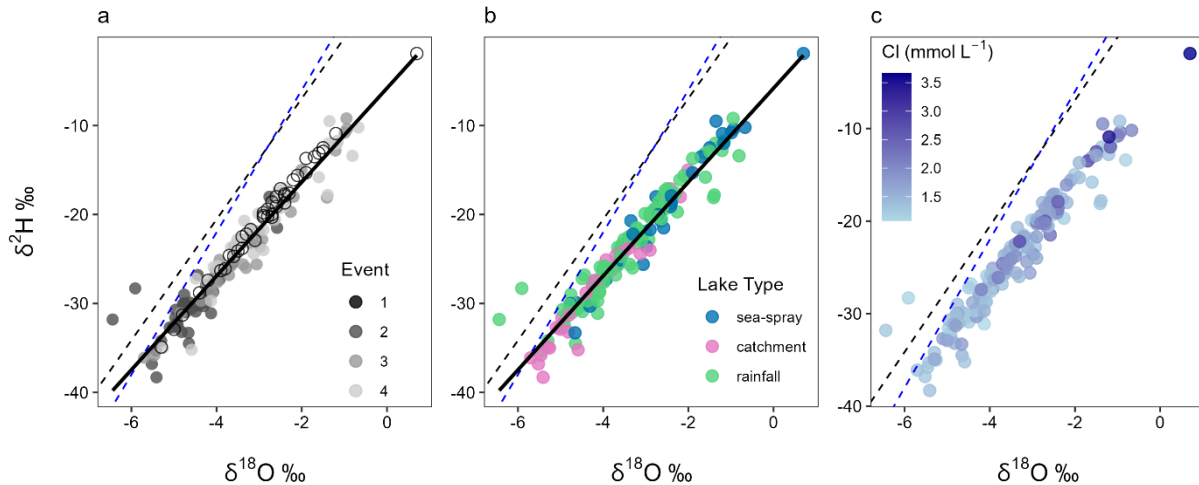


357  
 358 Fig. 5: Principal Component Analysis (PCA) of Macquarie Island lake waters, showing the relationships between major ions and  
 359 environmental parameters. Lakes are coloured by lake type, showing that lakes cluster based on the dominate geochemical  
 360 processes identified by Meredith et al., (2022). Dist. west coast = distance from the west coast (m), Conduct = electrical  
 361 conductivity.

### 362 3.2 Stable water isotopes

363  $\delta^2\text{H}$  and  $\delta^{18}\text{O}$  were measured in the 2022 samples and ranged from -38.3 to -9.2‰ and -38.3‰ to -  
 364 0.67‰, respectively. Lake waters in 2018 and 2022 fell below the Global and Cape Grim (northwest  
 365 Tasmania) Meteoric Water Lines (MWLs), suggesting slight isotopic enrichment in Macquarie Island's  
 366 lakes (Fig. 6). In 2018, lake waters were significantly higher in  $\delta^2\text{H}$  (mean -24.8 ‰) and  $\delta^{18}\text{O}$  (mean -  
 367 2.83‰) compared to 2022 (mean  $\delta^2\text{H}$  = -24.8 ‰ and  $\delta^{18}\text{O}$  = -3.55 ‰). Significant isotopic enrichment of  
 368  $\delta^2\text{H}$  and  $\delta^{18}\text{O}$  ( $p < 0.001$ ) can be seen in the data at the beginning of the 2022 austral summer (E2–3;  
 369 Fig. 6a). SSA influenced lakes tended to have higher isotopic values, while catchment influenced lakes

370 had lower values (Fig. 6b), with a significant difference between all lake types detected ( $p < 0.001$ ). LK20  
 371 and LK21 from E2 were outliers, plotting above the MWLs with lower  $\delta^{18}\text{O}$  values. Cl concentrations  
 372 appeared to be related to  $\delta^2\text{H}$  and  $\delta^{18}\text{O}$  values (Fig. 6c), however the correlation between the parameters  
 373 was low ( $R^2 \leq 0.24$ ). This lack of relationship was consistent across lake types and sampling events.



374  
 375 Fig. 6: Stable water isotope  $\delta^2\text{H}$  and  $\delta^{18}\text{O}$  differences in Macquarie Island lake waters, shown across: **a)** sampling events; **b)**  
 376 lake type; **c)**  $\delta^2\text{H}$  and  $\delta^{18}\text{O}$  relationship shown with Cl concentration ( $\text{mmol L}^{-1}$ ). Solid black line shows Macquarie Island  
 377 regression, blue dashed line is the Global Meteoric Water Line (GMWL:  $\delta^2\text{H} = 8 \delta^{18}\text{O} + 10$ ), and black dashed line is the Cape  
 378 Grim Local Meteoric Water Line (LMWL:  $\delta^2\text{H} = 6.8 \delta^{18}\text{O} + 6.65$ ).

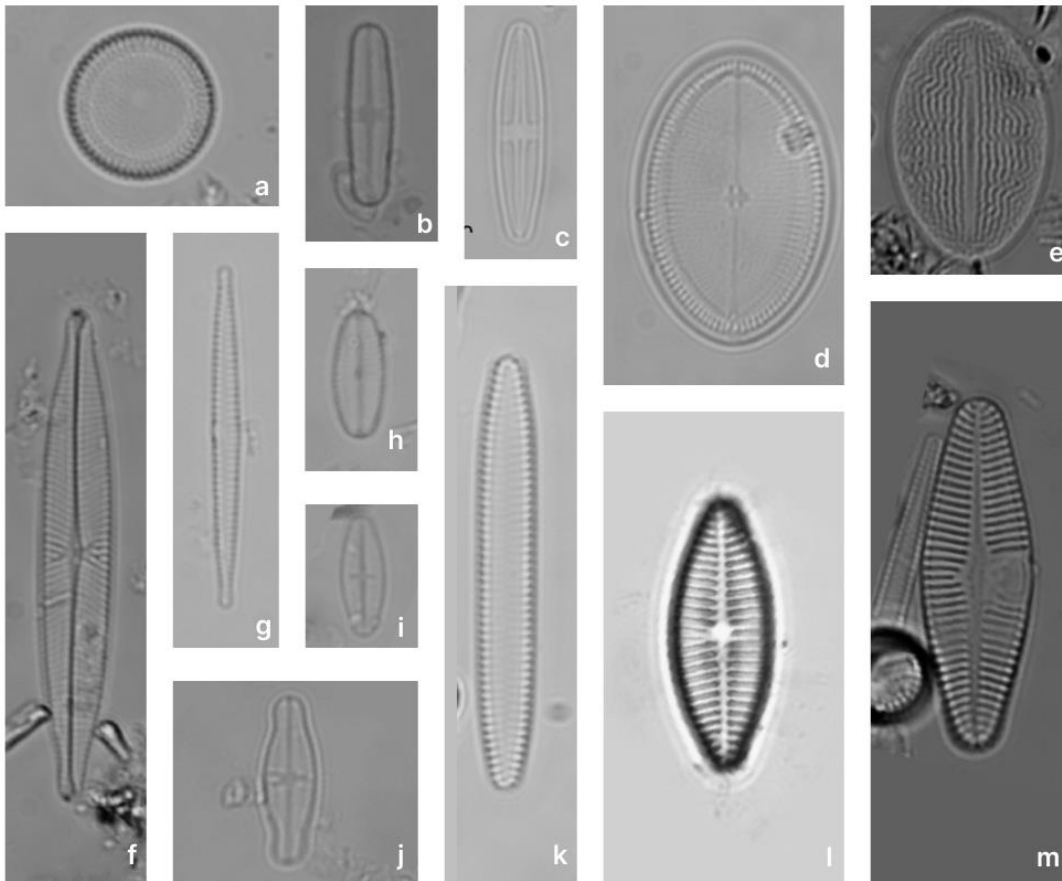
### 379 3.3 Diatoms

#### 380 3.3.1 Diatom communities

381 In total, 141 diatom taxa from 45 genera were identified in the 52 plateau and coastal lakes. Ninety-six  
 382 taxa (including 21 unknown species) from 30 genera remained in the dataset after taxa with  $\leq 1\%$  relative  
 383 abundance were excluded. The most taxon-rich genera were *Pinnularia* (16 taxa), *Psammothidium* (12  
 384 taxa), and *Planothidium* (8 taxa). The most dominant taxa being both common, occurring in  $>15$  lakes,  
 385 and abundant, occurring  $>25\%$  relative abundance in at least one sample, were *Aulacoseira principissa*  
 386 Van de Vijver, *Psammothidium abundans* (Manguin) Bukhtiyarova & Round, *Psammothidium confusum*  
 387 var. *atomoides* (Manguin) van de Vijver, unknown species 111, *Psammothidium confusum* (Manguin)  
 388 van de Vijver, *Fragilaria capucina* Desmazières, and *Navicula bergstromiana* Vyverman et al. Coastal  
 389 and plateau lakes showed distinctly different assemblages, with coastal lakes exhibiting less diversity  
 390 (mean number of species = 20) and dominated by taxa including *F. capucina*, unknown sp. 111,

391 *Planothidium quadripunctatum* (D.R.Oppenheim) Sabbe, *Planothidium delicatum* (Kützing) Round &  
 392 Bukhtiyarova, and *Planothidium lanceolatum* (Brébisson ex Kützing) Lange-Bertalot. Plateau lakes were  
 393 more diverse (mean number of taxa = 40) and dominated by *A. principissa*, *P. abundans*, *P. confusum*  
 394 var. *atomoides*, *P. confusum*, *N. bergstromiana*, *Achnanthisidium modestiformis* (Lange-Bertalot) Van de  
 395 Vijver, *Cocconeis placentulata* Ehrenberg, and unknown species 21. No taxa were found in all lakes,  
 396 and none were uniquely restricted to either coastal or plateau lakes, although clear differences in species  
 397 composition and relative abundance were observed. See Figure 7 for microscopy photos of the most  
 398 abundant taxa.

10µm



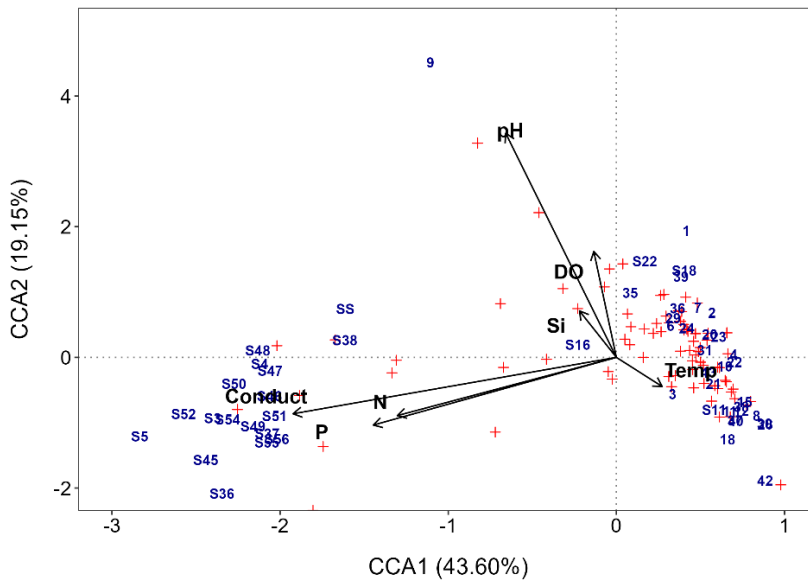
399  
 400 Fig. 7: The most abundant diatom taxa from plateau and coastal lakes on Macquarie Island. **a)** *Aulacoseira principissa*; **b)**  
 401 *Psammothidium abundans*; **c)** *Psammothidium confusum*; **d-e)** *Cocconeis placentulata*; **f)** *Navicula bergstromiana*; **g)** *Fragilaria*  
 402 *capucina*; **h)** Unknown species 21; **i)** *Psammothidium confusum* var. *atomoides*; **j)** *Achnanthisidium modestiformis*; **k)** Unknown  
 403 species 111; **l)** *Planothidium delicatum*; **m)** *Planothidium lanceolatum*.

404 **3.3.2 Diatom-environment relationships**

405 The full CCA model was significant ( $p = 0.001$ ), with environmental variables explaining 23.9% (Table 2)  
 406 of the total variance in diatom species composition (constrained inertia = 1.5). Together, the first two  
 407 canonical axes explained 62.8% of the total constrained variance (Table 2; Fig. 8). Forward selection  
 408 with Bonferroni corrections, identified EC, pH ( $p = 0.003$ ), and temperature ( $p = 0.015$ ) as the most  
 409 significant predictors of diatom community composition, collectively explaining 15.4% of the total  
 410 variance. This equates to 70% of the total explained variance in the full model, capturing the major  
 411 environmental gradients influencing species distribution with a more parsimonious model.

412 Table 2: Full CCA model results

Axis	Eigenvalue	Proportion of variance explained (%)	Cumulative proportion (%)
CCA1	0.77	51.07	51.07
CCA2	0.38	25.14	76.21
CCA3	0.22	14.55	90.76
CCA4	0.144	9.24	100.00
Constrained inertia	1.5		
Constrained proportion (%)	23.9		



413  
 414 Fig. 8: Full CCA ordination biplot of diatom species and environmental data, numbers indicate sites, and red symbols indicate  
 415 diatom species. Si = silicate, P = phosphate, N = total oxidised nitrogen, and conduct = electrical conductivity (EC).

416 Individual CCAs were performed to assess the total explanatory power of each variable. EC and pH were  
 417 shown to be the strongest, individually explaining 10.62% and 5.43% of the total variation, respectively.  
 418 This corresponds to 44.4% and 22.7% of the total variance in the full CCA model. Additionally, EC was  
 419 the only variable with a high  $\lambda_1/\lambda_2$  ratio ( $\lambda_1/\lambda_2 = 1.31$ ; Table 3), suggesting it is the only variable with  
 420 enough explanatory power for inference modelling.

421

422 Table 3: Individual CCA results, independent CCAs run for each variable. (\* = significant *p value* < 0.05)

Variable	$\lambda_1 / \lambda_2$	Constrained sum	Variance explained (%)	Proportion of full model explained (%)	p-value
Electrical conductivity	1.31	0.64	10.62	42.28	0.001*
Phosphate	0.73	0.40	6.59	26.23	0.001*
Total oxidised nitrogen	0.68	0.35	5.78	22.99	0.001*
pH	0.39	0.33	5.43	21.63	0.001*
Silicate	0.26	0.19	3.14	12.48	0.034*
Temperature	0.22	0.14	2.27	9.03	0.382
Dissolved oxygen	0.12	0.12	1.97	7.85	0.586

423

424 Partial CCAs were performed with each environmental variable tested separately while controlling for  
 425 covariation with all other variables, to quantify unique and shared variance contributions. EC, pH, and Si  
 426 were the only variables to have significant unique contributions ( $p \leq 0.01$ ; Table 4). The shared and  
 427 unique variance of each environmental variable is shown in Figure 9. EC explained the largest proportion  
 428 of total constrained variation (46%) in diatom community composition, with a large shared component  
 429 (18% unique, 28% shared), suggesting it acts along a major environmental gradient shared with TON  
 430 and  $\text{PO}_4^{3-}$  (Fig. 8). Despite this, it performed well in all other CCAs and its unique contribution remained  
 431 high, indicating it is an important independent driver of diatom structure across Macquarie Island lakes.  
 432 Furthermore, low VIFs among all environmental variables (VIFs <3) indicated that multicollinearity was  
 433 low. EC (VIF = 2.6) showed a low correlation with other variables ( $R^2 \leq 0.47$ ), suggesting it represents a  
 434 largely independent gradient in the dataset. In contrast, pH had similar unique variance (18.4%) and  
 435 lower shared variance (2.4%), implying a more independent ecological influence.

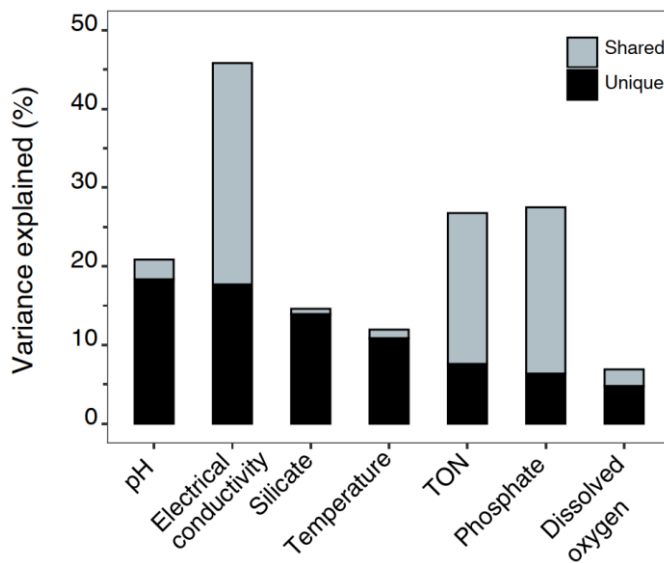
436

437

438

439 Table 4: Partial CCA results, where each variable was tested with the covariation of other variables controlled (\* = significant  $p$   
 440  $value < 0.05$ ).

Variable	Variance explained (%)	Proportion of full model explained (%)	p-value
pH	5.97	18.92	0.001*
Electrical conductivity	5.58	17.62	0.001*
Silicate	3.87	11.99	0.008*
Temperature	2.81	8.61	0.151
Total oxidised nitrogen	2.06	6.28	0.651
Phosphate	1.71	5.20	0.774
Dissolved oxygen	1.34	4.06	0.991



441  
 442 Fig. 9: Variance partitioning showing unique and shared proportions of variance explained by each environmental variable.

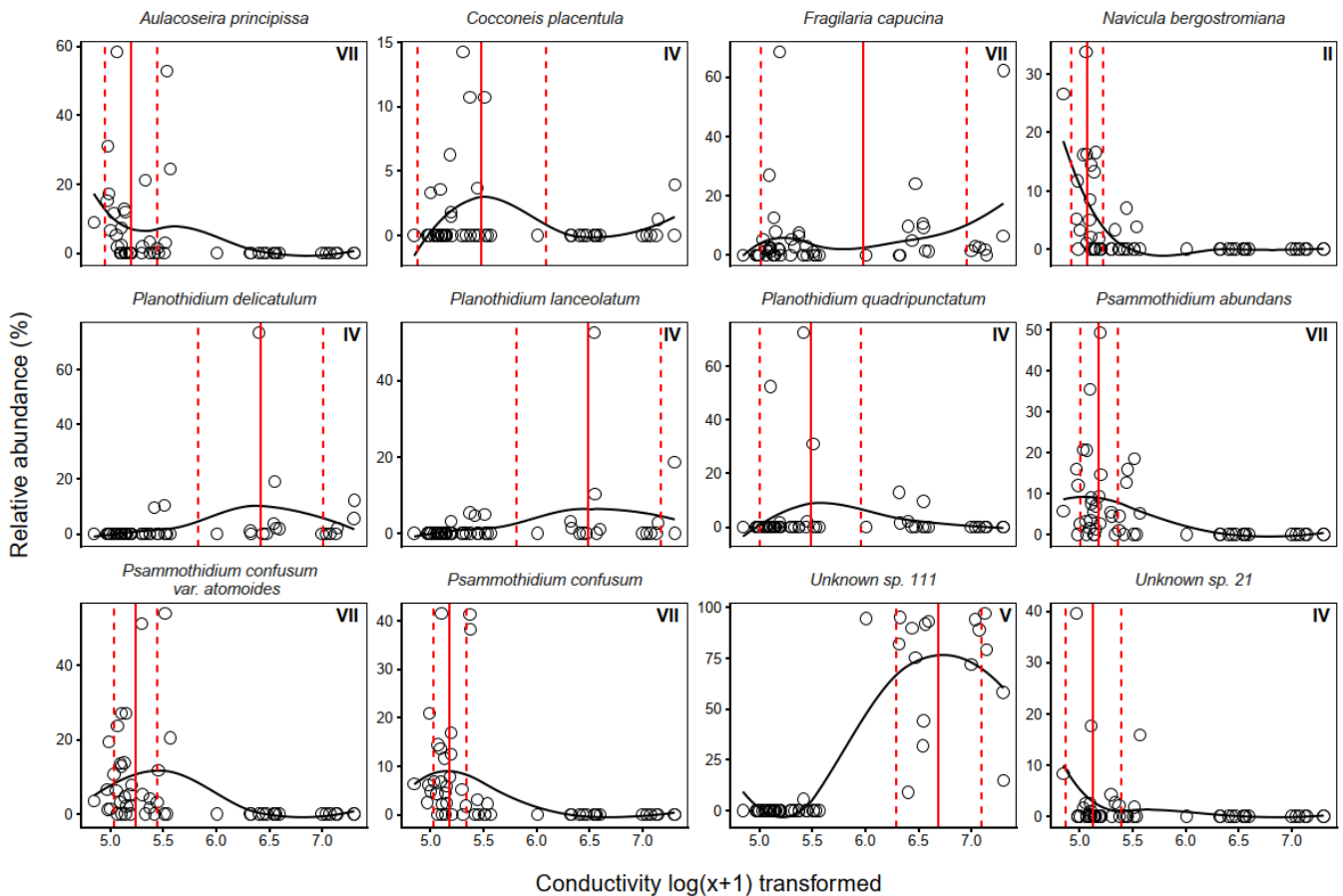
### 443 3.3.3 Species optima and tolerances

444 Species optima across major environmental gradients EC and pH were determined with WA. *F.*  
 445 *capucina*, *P. lanceolataum*, and *P. delicatulum* were found across the EC range with broad tolerances,  
 446 however each species showed different optima (Fig. 10). The apparent bimodal distribution of *F.*  
 447 *capucina* likely reflects ecological plasticity across differing hydrochemical conditions and/or potential  
 448 taxonomic aggregation within this morphotype. Exploration of a GAM-based response curve (Fig. S2)  
 449 indicates *F. capucina* has a weak non-linear relationship with EC, suggesting a broad and flexible

450 ecological response rather than a strongly defined unimodal optimum. Unknown sp. 111 was found to  
 451 tolerate high EC, while most other dominant species, including *A. principissa*, *C. placentulata*, *N.*  
 452 *bergstromiana* and dominant *Psammothidium* species show tolerance and optima for low EC.

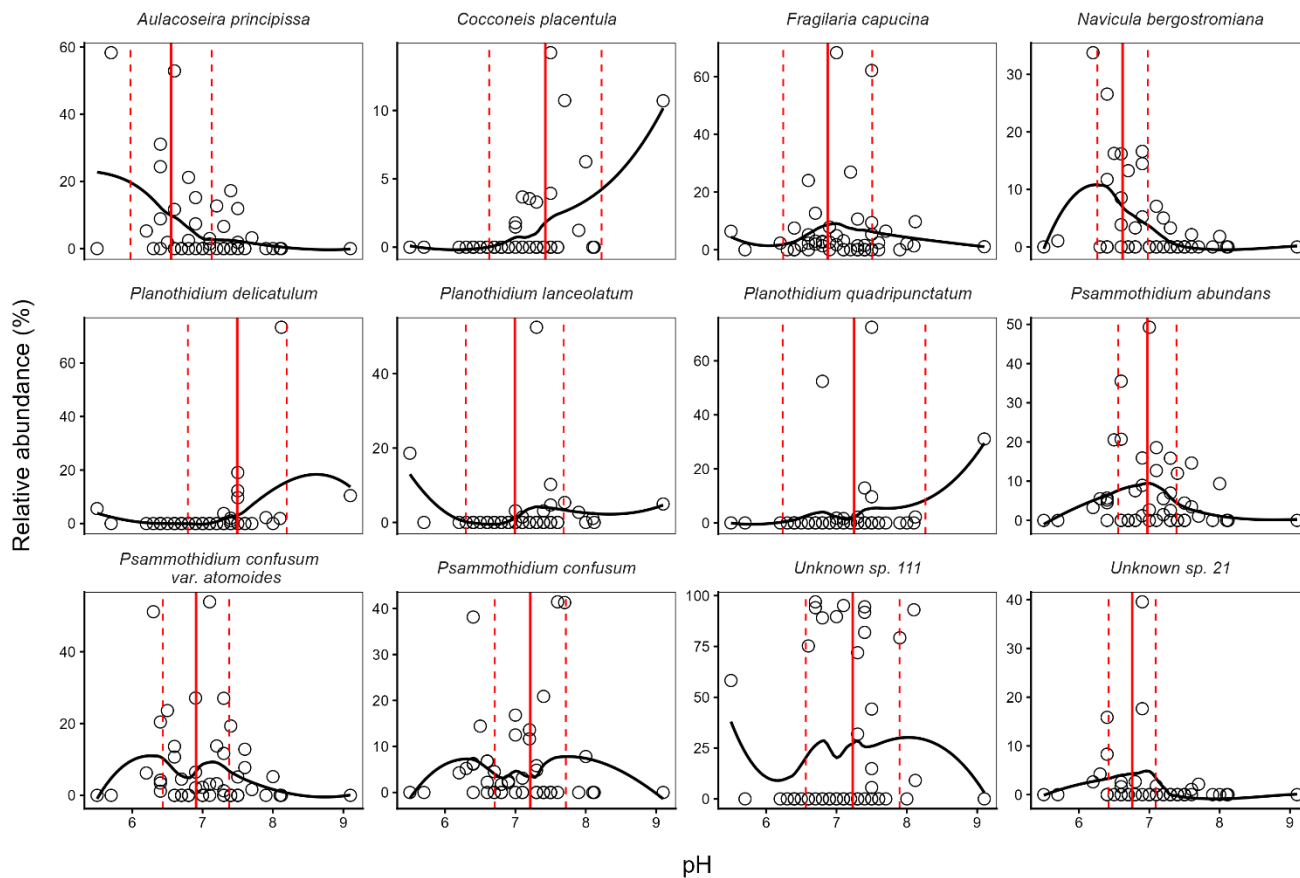
453

454 Dominant diatom species occurred across the pH gradient, with species optima ranging from moderately  
 455 acidic to neutral (Fig. 11). Most dominant species had optima for moderate acidity, with *Psammothidium*  
 456 species, *A. principissa*, and *N. bergstormiana* showing narrow pH tolerances. *C. placentulata* and *F.*  
 457 *capucina* showed broader tolerances and unknown sp. 111 was the only dominant species with a near  
 458 neutral optima.



459

460 Fig. 10: Weighted averaging (WA) optima (solid red line) and tolerance ranges (dashed red lines) for dominant diatom species  
 461 across the electrical conductivity gradient in Macquarie Island lakes. Observed relative abundances (%) are plotted against log-  
 462 transformed electrical conductivity, with fitted loess curves illustrating species response shapes along the conductivity gradient  
 463 (126–1482  $\mu\text{S}/\text{cm}$ ). Roman numerals indicate Gaussian response curve type.



464

465 Fig. 11: Weighted averaging (WA) optima (solid red line) and tolerance ranges (dashed red lines) for dominant diatom species  
 466 across the pH gradient in Macquarie Island lakes. Observed relative abundances (%) are plotted against pH, with fitted loess  
 467 curves illustrating species response shapes along the pH gradient (5.50–9.14°C).

### 468 3.3.4 Diatom transfer functions

469 Ordination analyses showed that EC and pH explained significant and independent proportions of  
 470 variance in diatom composition. While temperature also showed significant but lesser contributions, it  
 471 was not considered for transfer function development as diatom-based temperature reconstructions as  
 472 species responses to temperature can be indirect and influenced by multiple co-varying environmental  
 473 gradients, limiting the reliability of temperature inference (e.g. Juggins, 2013). While Si was shown to  
 474 independently contribute to diatom variance, reduced CCA modelling with forward selection did not  
 475 indicate it to be a major environmental gradient. Transfer functions were therefore only developed for EC

476 and pH. Transfer function results for the best performing WA, WAPLS, or ML model for EC and pH are  
477 described in Table 5.

478  
479 Table 5: Best performing WA, WAPLS or ML model results for electrical conductivity and pH.

Variable	Model	$R^2$	$R^2_{boot}$	RMSE	RMSEP
Electrical conductivity	WA <sub>inv</sub>	0.83	0.74	0.31	0.39
	ML	0.91	0.80	0.22	0.40
pH	WAPLS-2	0.72	0.26	0.33	0.60

480

481 For EC, WA<sub>INV</sub> and WAPLS-1 produced near identical results. WA<sub>INV</sub> was favoured as the simpler model  
482 (WA<sub>INV</sub>,  $R^2= 0.83$ ,  $R^2_{boot}= 0.74$ , RMSE = 0.31, RMSEP = 0.39). Although WAPLS-2 to -5 increased  $R^2$   
483 and reduced RMSE, each successive component progressively increased RMSEP by 13-16%, thereby  
484 reducing performance. Given the unimodal gradient structure of the dataset, ML modelling was also  
485 assessed for EC. ML showed slightly stronger predictive performance to WA<sub>INV</sub>, with higher  $R^2_{boot}$  and  
486 comparable RMSEP (ML,  $R^2= 0.91$ ,  $R^2_{boot}= 0.80$ , RMSE = 0.23, RMSEP = 0.40).

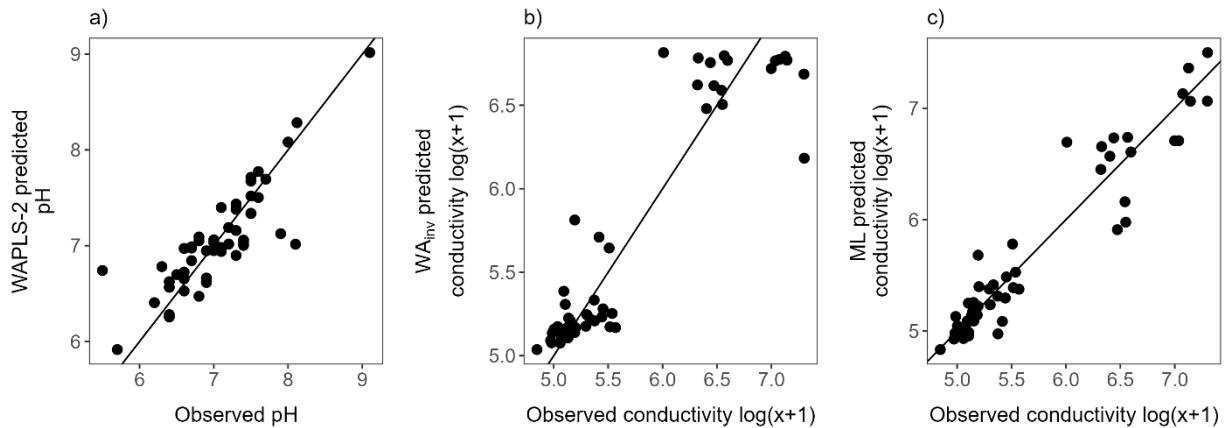
487

488 Comparison of observed and predicted value scatter plots indicated that ML achieved a tighter fit, with  
489 WA<sub>INV</sub> showing increased predictive error at higher EC ranges (Fig. 12). However, further inspection  
490 indicated that only ~30% of taxa displayed Gaussian (Type IV–V) response curves indicating ML may  
491 not be the most appropriate approach (Fig. 10 and see Table S5 for full Gaussian response curve  
492 results). However, overfitting from ML is not likely as RMSEP did not increase. Overall, both models  
493 show cross-validated performance and are considered robust.

494

495 pH had poor performance across all WA and WAPLS models with high RMSEP ( $\geq 0.6$ ) and low  $R^2_{boot}$  ( $\leq$   
496 0.26). WAPLS-2 was found to be the strongest model (WAPL-2,  $R^2= 0.72$ ,  $R^2_{boot}= 0.26$ , RMSE = 0.33,  
497 RMSEP = 0.60). ML modelling showed poor performance for pH with high RMSEP = 0.93.

498



499

500 Fig. 12: Comparison of observed environmental measurements with values predicted by diatom-based transfer functions: **a)** pH estimated using  
 501 WAPLS-2; **b)** conductivity estimated using WA with inverse deshrinking (WA<sub>inv</sub>); and **c)** conductivity estimated using the maximum likelihood  
 502 (ML) method. Black lines show the 1:1 line.

## 503 4 Discussion

### 504 4.1 Annual and seasonal lake water hydrogeochemical variation

505 The seasonal hydrochemistry dataset presented in this study support the 2018 baseline assessment  
 506 (Meredith et al., 2022) that lake water chemistry is controlled by SSAs, terrestrial catchment processes,  
 507 elevation and rainfall dilution. The seasonal water chemistry data, which is presented for the first time in  
 508 this study, shows that there is no significant variation in major ions across the 2022–23 austral summer.  
 509 Comparison of 2018 and 2022 data shows that significant variation ( $p < 0.005$ ), in some major ions is  
 510 evident, with higher concentrations in 2018 of Br and Cl, SO<sub>4</sub>, and Mg associated with SSAs. Although  
 511 not statistically significant ( $p > 0.005$ ), other sea-spray derived ion mean values (Na, Ca, K) were higher  
 512 in 2018 (Fig. 3; Table S4). However, not all ions increased in concentration, and terrestrially derived ions  
 513 such as Fe, F, Si, and Al were lower in 2018, suggesting that lakes in 2022 had stronger SSA influence.  
 514

515 Despite these changes, PCA of the 2018 and 2022 lake water chemistry datasets (Fig. 5) show that  
 516 lakes typically cluster by the lake types identified in Meredith et al. (2022) (i.e., as SSA, catchment and  
 517 rainfall influenced). This indicates that the major hydrogeochemical processes influencing Macquarie  
 518 Island lakes are consistent between years, with no major environmental shifts occurring in weathering  
 519 and erosion of the island's geology, suggesting these processes are stable on an annual time scale.

520 Identifying hydrogeochemical stability is important for identifying lake sites suitable for diatom–  
521 conductivity inference models. It also strengthens palaeoclimate interpretations by suggesting that local  
522 lake dynamics are relatively constant, supporting the hypothesis that in sea-spray dominated lakes,  
523 proxies primarily record externally forced changes driven by the SHW rather than internal hydrological  
524 or geochemical dynamics (Saunders et al. 2018; Perren et al. 2020). This further emphasises that water  
525 chemistry characteristics are critical to consider in site-selection to develop reliable SHW reconstructions  
526 on Macquarie Island.

## 527 **4.2 Evaporation**

528 Interpreting environmental proxies as direct indicators of climate variability can be challenging, as  
529 multiple processes may produce similar signals (Molén 2024). When using diatom–conductivity models  
530 to infer past SHW variability, it is essential to consider how near surface evaporation has the potential to  
531 concentrate ions in surface waters and mimic the effects of other processes such as increasing lake  
532 water salinity from SSA deposition due to stronger winds. Although this study and previous studies  
533 (Evans 1970; Buckney and Tyler 1974; Meredith et al. 2022) have demonstrated that SHW-driven SSA  
534 inputs are a dominant control on lake water chemistry on Macquarie Island, the role of evaporation in  
535 amplifying these signals remains unclear.

536

537 To explore this, we analysed  $\delta^2\text{H}$  and  $\delta^{18}\text{O}$  values from 2018 and across the 2022–23 Austral summer.  
538 Isotopic enrichment is evident across the 2022–23 season (Fig. 6a), indicating a strengthening  
539 evaporative signal through summer. Lake stable water isotopes sampled in 2018 were significantly more  
540 enriched than the 2022 mean, as expected given that the 2018 samples were collected in late summer,  
541 when evaporative effects are strongest and cumulative due to warmer temperatures throughout summer.  
542 This is supported by lake water temperatures being significantly lower in early summer (E2) compared  
543 to late summer (E3 and E4; Table 1). Given Macquarie Island’s persistently high cloud cover, humidity,  
544 and low sunshine hours (BOM, 2025), solar evaporation is likely limited and confined to the summer  
545 season. Evaporation can produce heavy-isotope enrichment and the residual lake water becomes  
546 progressively enriched in heavier isotopes ( $\delta^2\text{H}$  and  $\delta^{18}\text{O}$ ), moving away from the Global MWL (Gat 1996).  
547 Comparisons between E1 (2018) and E4 (2022), which were sampled at the same time of the year in  
548 January–February provide a valuable comparison of potential interannual variability in lake water  
549 chemistry and processes (Fig. 3, Table S4). These two sampling events show near identical mean

550 isotopic composition ( $p > 0.01$ ;  $\delta^2\text{H} = -20.7\text{‰}$  and  $\delta^{18}\text{O} = -2.8\text{‰}$  in 2022, and  $\delta^2\text{H} = -20.1\text{‰}$  and  $\delta^{18}\text{O} = -$   
551  $2.8\text{‰}$  in 2018), suggesting broadly stable summer evaporative conditions between years. Furthermore,  
552 SSA influenced lakes on the plateau are in proximity to the west coast and have the greatest exposure  
553 to the SHW (Fig. 2b). These lakes have significantly higher isotopic enrichment (Fig. 5b), providing  
554 further evidence that wind is likely the primary driver of evaporation in plateau lake waters across  
555 Macquarie Island, particularly in lakes located on the west coast, which may be most suitable for  
556 reconstructions of SHW dynamics (Saunders et al., 2018). As both wind-enhanced evaporation and  
557 wind-driven SSA transport and deposition contributes to the concentration of SSA ions in these lakes,  
558 both ion deposition and concentration reflect a SHW signal.

559

560  $\text{Cl}^-$  is a robust tracer of hydrogeochemical processes and, together with  $\delta^2\text{H}$  and  $\delta^{18}\text{O}$  values, can be  
561 used to better understand evaporation (Kirchner et al., 2010). While the isotopic enrichment observed  
562 generally indicates an evaporative signal, the absence of a correlation between  $\text{Cl}^-$  and  $\delta^2\text{H}$  or  $\delta^{18}\text{O}$  (Fig.  
563 6c) suggests that isotopes are capturing short-term (summer) evaporation rather than sustained  
564 evaporative concentration sufficient to increase  $\text{Cl}^-$  concentration in the lake waters like those in  
565 environments driven primarily by solar evaporation (Meredith et al. 2009). On Macquarie Island, wind-  
566 driven SSA deposition and rainfall dilution therefore likely remain the primary drivers of  $\text{Cl}^-$  variability.  
567 Consequently, EC in lake waters of Macquarie Island remains a robust proxy for interpreting variations  
568 in SHW strength.

### 569 **4.3 Diatom communities**

570 Diatom analysis showed that typical sub-Antarctic genera (Van de Vijver 2019; Goeyers et al. 2022),  
571 including *Psammothidium*, *Planothidium*, and *Fragilaria*, dominated lake diatom communities on  
572 Macquarie Island. Across 52 lakes, 141 taxa were identified, indicating intermediate species diversity  
573 relative to previous studies on the island which reported 102 (McBride, 2009) and 208 (Saunders et al.,  
574 2009) species. Consistent with these earlier studies we have demonstrated that diatoms on Macquarie  
575 Island exhibit clear and distinct ecological preferences. Combined with the pronounced environmental  
576 gradients among lakes, these species-environment relationships provide a strong basis for using diatoms  
577 as indicators of limnological conditions and environmental change.

578

579 *Psammothidium* species are characteristic of low EC sites (Van de Vijer et al. 2002), and while  
580 abundance and dominance of key *Psammothidium* species showed variation along the lower end of the  
581 EC gradient (Fig. 10), they dominated low EC sites. *N. bergstromiana* is considered endemic to  
582 Macquarie Island and was commonly found with dominant *Psammothidium* species at low EC sites,  
583 typically occurring where EC was  $<200 \mu\text{S cm}^{-1}$ , consistent with what has previously been reported  
584 (Sabbe et al. 2019). *A. principissa*, previously identified as *Aulacoseria distans* (Ehrenberg) Simonsen  
585 on Macquarie Island (McBride, 2009; Saunders et al., 2009), was also common at low EC (Fig. 10). This  
586 taxa is commonly found on sub-Antarctic Islands and is suggested to prefer very low conductance values  
587  $<80 \mu\text{S cm}^{-1}$  (Van de Vijver 2012), while EC was not observed  $<160 \mu\text{S cm}^{-1}$  in this dataset, *A. principissa*  
588 may be an indicator of very low EC conditions.

589

590 *P. lanceolatum* was a dominant high EC, high nutrient taxa. While it has been found to dominate flora  
591 elsewhere, this contrasts previous studies where it has been reported to be characteristic of oligotrophic  
592 conditions (Van de Vijer et al. 2002). *F. capucina*, *P. delicatulum*, and unknown sp. 111 were more  
593 commonly dominant at high EC. *F. capucina* was found across the EC gradient displaying a bimodal  
594 distribution (Fig. 10), consistent with its cosmopolitan and ecologically tolerant nature (Van de Vijer et  
595 al., 2002).

#### 596 **4.4 Developing transfer functions**

597 A key aim of this study was to update and improve existing quantitative diatom models for Macquarie  
598 Island. While the dominant taxa identified here are consistent with those reported by Saunders et al.  
599 (2009), the strength of some diatom–environment relationships differ. EC and pH remain strong  
600 explanatory variables for diatom variation, whereas  $\text{PO}_4^{3-}$  and Si showed limited influence in the present  
601 study (Table 3 and 4). This reduced explanatory power likely reflects the low nutrient variability across  
602 plateau lakes, where concentrations were generally below detection limits.

603

604 Sub-Antarctic lakes are characteristically oligotrophic; high nutrient levels do occur, but they are  
605 associated with peatlands or animal colonies, as is the case with coastal lakes on Macquarie Island  
606 (Selkirk et al. 1990). Saunders et al. (2009) recorded greater nutrient variability across plateau sites at  
607 the lower end of the EC gradient, attributed to enhanced organic inputs during periods of high ecological  
608 disturbance from invasive rabbits. These differences suggest that the dataset in the present study

609 represents post-eradication limnological conditions that are more reflective of pre-invasion or near-  
610 natural states, providing an updated basis for developing robust diatom–environment models that are  
611 less influenced by disturbance. The use of field parameters collected across multiple sampling events  
612 increases confidence that the developed models reflect representative environmental conditions  
613 (Goldenberg Vilar et al. 2018; Kennedy and Buckley 2021). Such repeated-sampling approaches are  
614 rarely achieved in diatom transfer function development, particularly in remote regions such as the sub-  
615 Antarctic.

616

617 Widespread recovery of vegetation communities provides evidence for catchment scale ecosystem  
618 recovery across the island (Springer 2018; Fitzgerald et al. 2021). While quantitative runoff or nutrient  
619 time series are not available to directly extend this to limnological conditions, we are able to provide site-  
620 specific evidence from one sedimentary diatom record. At Emerald Lake (LK6), downcore diatom  
621 assemblages show a clear ecological shift coincident with the introduction of rabbits (1878 CE) and their  
622 establishment on Macquarie Island, with *F. capucina* and *P. abundans* dominating downcore intervals  
623 (Saunders et al. 2013). In contrast, diatom assemblages in recent (2022) surface sediments from this  
624 site exhibit higher diversity (48 species) and greater similarity in assemblage composition to pre-rabbit  
625 sediment intervals rather than assemblages from previously collected 2006 surface sediments (15  
626 species), which were dominated by *F. capucina* (48% relative abundance). Notably, *F. capucina* was  
627 absent from the 2022 surface sample. Together, these lines of evidence suggest that the modern  
628 calibration dataset is less influenced by organic inputs and erosion associated with the rabbit invasion  
629 period. Accordingly, we interpret the 2022 dataset as representing post-eradication recovery conditions  
630 that are moving toward, but do not necessarily fully reflect, pre-disturbance baseline states. However,  
631 further studies are needed to assess how widespread this is across the island.

632

633 EC was shown to be the major independent driver of diatom assemblages, with strong performance in  
634 all CCA models, individually accounting for almost 50% of the variance in the full CCA model and strong  
635 explanatory power as indicted by  $\lambda_1/\lambda_2$  (Table 3). Although EC reflects a high proportion of shared  
636 variance (Fig. 9), this is consistent with its role as an integrative measure of ionic strength and catchment  
637 inputs. The shared component primarily reflects its covariation with major ions and nutrient variables  
638 (TON and  $\text{PO}_4^{3-}$ ), which are typically correlated with EC in these systems. Despite this overlap, EC

639 retained a strong and highly significant independent effect ( $p = 0.001$ ), confirming its dominant ecological  
640 influence on diatom distributions.

641

642 While  $\text{PO}_4^{3-}$ , TON, and Si each explained significant but moderate portions of individual variance (Table  
643 3), they were no longer significant once covariation was controlled for (Table 4), meaning their  
644 explanatory power is mostly shared variance with other environmental gradients, primarily EC and each  
645 other, with negligible unique variance. This interpretation is supported by simple linear correlations  
646 between EC and nutrient variables in coastal lakes, which show weak or absent relationships (Fig. S3).  
647 These results indicate that although nutrients and EC co-occur in coastal systems, nutrient variability is  
648 not strongly or systematically coupled to EC. Together with the VIFs ( $<3$ ), variance partitioning and partial  
649 CCA results (Table 4), this supports the interpretation that the weak unique nutrient signal reflects an  
650 ecological reality in which EC exerts a first-order control on diatom assemblages, rather than a statistical  
651 artefact of collinearity. Similarly, while pH explained a major and independent gradient in diatom variation  
652 within plateau lakes (Fig. 8), it did not capture assemblage changes across high-EC, high-nutrient sites.  
653 This was indicated by individual CCA results, which were less than half of the variance explained by EC  
654 (Table 3). This, paired with the widespread oligotrophic nature of plateau lakes on Macquarie Island  
655 lends strength to the independent explanatory power of EC across the whole dataset.

656

657 Furthermore, pH showed poor predictive performance as a transfer function, with the lowest  $R_{boot}^2 = 0.26$ ,  
658 and high RMSEP = 0.6 from the WAPLS-2 model (Table 5). While this is surprising due to the strong pH  
659 gradient across plateau sites, most diatoms were found across the pH gradient (Fig. 11) with some  
660 species showing broad tolerance and pH ranges. EC had the strongest performance with the WA and  
661 ML models producing the highest  $R_{boot}^2$  (0.74 and 0.80, respectively) and comparable RMSEP.  $\text{WA}_{inv}$   
662 and WAPLS-1 showed identical performance, with no benefit from additional WAPLS components, which  
663 progressively increased predictive error and decreased  $R_{boot}^2$ , suggesting overfitting. WA was therefore  
664 chosen over WAPLS as the simpler model.

665

666 The WA EC transfer function performed better than the previously published Macquarie Island diatom-  
667 conductivity transfer function (Saunders et al., 2009), with higher  $R_{boot}^2$ . However, some caution is  
668 warranted when predicting across the upper EC range, where greater predictive error is evident (Fig.

669 12). This can be attributed to lower species turnover, higher variability in  $\text{PO}_4^{3-}$ , TON, and Si, and fewer  
670 sites at the upper end of the nutrient and EC gradients. Further refinement of the EC transfer functions  
671 could be achieved with more evenly distributed sampling across the environmental gradient. The ML  
672 model, with higher  $R_{boot}^2$ , appears more capable of addressing these issues and maintains more  
673 consistent predictive power across the EC range. This is likely due to its explicit curve-fitting approach.  
674 By estimating individual species optima and tolerances, ML can better represent asymmetric or skewed  
675 response curves (Birks 2012). The ML transfer function is therefore considered to be the preferred model,  
676 although both WA and ML are robust based on comparable RMSEP.

#### 677 **4.5 Future applications for reconstructing past climate changes**

678 The conceptual link between large-scale wind regimes and long-term limnological and ecological  
679 responses in Southern Hemisphere lake systems is well established in previous studies (e.g., Saunders  
680 et al. 2009; 2016; 2018; Perren et al. 2020, 2025; Van Nieuwenhuyze 2020; Humphries et al. 2021;  
681 Meredith et al. 2022). The data presented here builds on this existing framework and demonstrates that  
682 incorporating diatom data with seasonal and multi-year hydrogeochemical data provides a unique  
683 opportunity to comprehensively understand diatom-environment responses. By quantifying temporal  
684 variability in hydrogeochemical processes, including the role of evaporation, this study strengthens  
685 confidence that EC reflects SHW-driven sea-spray inputs rather than local lake hydrogeochemical  
686 processes. This hydrological context is critical for interpreting diatom-environment relationships and  
687 ensuring the reliability of EC as a proxy for past SHW behaviour, providing a strong foundation for future  
688 palaeoclimate reconstructions. The resulting diatom-conductivity model provides a robust and  
689 ecologically grounded framework for reconstructing long-term SHW variability on Macquarie Island and  
690 establishes an important benchmark for sub-Antarctic palaeoclimate comparisons across the region.  
691 This model will be applied in future studies to reconstruct past variability in the SHW and associated  
692 hydroclimatic changes on Macquarie Island. Any future time-series monitoring of lake EC paired with  
693 local wind speed records would further allow direct assessment of the relationship between wind speed  
694 and lake salinity, including the rate of hydrogeochemical response and any wind speed thresholds  
695 required to drive measurable change.

696

697 By capturing post-eradication and near-natural ecological conditions, the EC model developed in this  
698 study offers an improved foundation for assessing long-term wind-driven variability, as it reduces

699 ecological noise associated with past disturbance. When applied in parallel with other proxies, such as  
700 isotopic or geochemical indicators, these reconstructions will contribute to a more comprehensive  
701 understanding of past SHW dynamics and their role in modulating Southern Hemisphere mid-high  
702 latitude climate, thereby providing context for understanding future changes.

703

704 Furthermore, a multiproxy approach will be valuable for independently reconstructing key climatic  
705 drivers, including precipitation, temperature, and atmospheric circulation, thereby improving  
706 interpretations of past SHW variability and helping to assess how hydroclimatic processes may modify  
707 EC signals (e.g., through dilution and enrichment). On Macquarie Island, geochemical indicators of sea-  
708 spray and dust inputs (e.g., S, Br, Ti) can help distinguish marine aerosol delivery from catchment-  
709 derived material, while glycerol dialkyl glycerol tetraethers (GDGT)-biomarker reconstructions can  
710 provide an independent constraint on temperature variability. Both approaches are currently being  
711 undertaken on Macquarie Island lake sediment cores by our research group. Mercury (Hg)  
712 concentrations and isotopes offer an independent proxies for atmospheric transport and Hg deposition  
713 linked to large-scale circulation, precipitation, and the influence of seabirds, all particularly well suited to  
714 the remote setting of Macquarie Island (Schneider et al., 2022; Guédron et al., 2020), which is also the  
715 focus of ongoing work (e.g. Schneider et al., 2024; Li et al., 2025). Although isotope ( $\delta^2\text{H}$ ,  $\delta^{18}\text{O}$ ) palaeo-  
716 records are not currently available for Macquarie Island, they represent an important avenue for future  
717 research to constrain precipitation–evaporation balance. Together, these complementary proxies  
718 provide a framework to separate the relative influence of atmospheric circulation, hydroclimate, and  
719 temperature on lake systems, providing more comprehensive palaeoclimate records and interpretations.

## 720 **5 Conclusion**

721 This study aimed to update and re-evaluate the reliability of diatom–conductivity models as a proxy for  
722 reconstructing SHW variability on Macquarie Island by analysing diatom–environment relationships in  
723 the context of seasonal and multi-year water chemistry and isotopic analyses. Our results demonstrate  
724 that although lake hydrogeochemical processes vary locally, they remain stable seasonally and between  
725 years. Lakes near the west coast and on the western edge consistently reflect strong SSA influence, and  
726 while short-term evaporative enrichment occurs during summer, it does not obscure the dominant signal  
727 of SHW-driven SSA inputs. Accordingly, EC reliably reflects SSA deposition rather than internal lake

728 hydrogeochemical processes, providing a firm mechanistic basis for the use of EC as an indicator of  
729 SSA deposition in palaeoclimate studies on Macquarie Island.

730

731 Diatom–environment relationships were found to be strong and ecologically coherent, supporting the  
732 development of a robust diatom–conductivity transfer function. Importantly, this study highlights the need  
733 for careful site selection, with lakes that demonstrate stable hydrogeochemical behaviour, clear SSA  
734 influence, and limited local disturbance providing the most reliable archives for reconstructing past SHW  
735 variability. The resulting EC transfer function offers a reliable tool for reconstructing long-term SHW  
736 dynamics, supported by well-characterised modern hydrological controls. Together, these findings  
737 establish Macquarie Island as a well-constrained system for SHW reconstructions and provide a strong  
738 foundation for future palaeoclimate work across the sub-Antarctic region.

739

#### 740 **Supplementary material**

741 The Diatom Catalogue and Species List can be accessed from DOI [10.5281/zenodo.18041221](https://doi.org/10.5281/zenodo.18041221)

742

#### 743 **Data availability**

744 The raw data supporting the conclusions of this work is available on request.

745

#### 746 **Author contributions**

747 Caitlin Selfe: Conceptualization; Data curation; Formal analysis; Investigation; Methodology; Validation;  
748 Visualization; Writing - original draft; Writing - review & editing.

749 Karina Meredith: Supervision; Research design; Resources; Writing - review & editing

750 Liza McDonough: Resources; Writing - review & editing

751 Justine Shaw: Supervision; Writing - review & editing

752 Stephen Roberts: Supervision; Writing - review & editing

753 Krystyna Saunders: Conceptualisation; Supervision; Resources; Funding acquisition; Writing - review  
754 & editing

755 Competing interests: The contact author has declared that none of the authors has any competing  
756 interests.

757

758

## 759 **Acknowledgments**

760 This work was supported by ARC SRIEAS Grant SR200100005 Securing Antarctica's Environmental  
761 Future. CS was supported by an AINSE Ltd. Residential Student Scholarship and acknowledges help  
762 undertaking fieldwork from Maggie Smith, Sam Beale, Jez Bird, and Adam Darragh. We thank the  
763 Tasmanian Parks and Wildlife Service and Australian Antarctic Division (AAS 4628) for field support  
764 and access to Macquarie Island. We also thank ANSTO laboratories for sample analysis, particularly  
765 Chris Vardanega and Henri Wong. This work contributes to delivering the Australian Antarctic Science  
766 Decadal Strategy, in particular the Climate System and Change key priority.

## 767 **References**

- 768 Andersen, T., J. Carstensen, E. Hernandez-Garcia and C. M. Duarte. Ecological thresholds and regime shifts: approaches to  
769 identification, *Trends Ecol. Evol.*, 24 (1), 49-57, 2009.
- 770
- 771 Birks, H., D. Frey and E. Deevey. Numerical tools in palaeolimnology-progress, potentialities, and problems, *J. Paleolimnol.*,  
772 20, 307-332, 1998.
- 773
- 774 Birks, H. J. B.: Overview of numerical methods in palaeolimnology, In: *Tracking environmental change using Lake sediments:*  
775 *Data handling and numerical techniques*, Springer, 19-92, 2012.
- 776
- 777 BOM. Australian Bureau of Meterology, Climate statistics for Australian locations.  
778 [https://www.bom.gov.au/climate/averages/tables/cw\\_300004.shtml](https://www.bom.gov.au/climate/averages/tables/cw_300004.shtml). 2025.
- 779
- 780 Buckney, R. T. and P. A. Tyler. Reconnaissance limnology of Sub-Antarctic islands. II. Additional features of the chemistry  
781 of Macquarie Island lakes and tarns, *Mar. Freshw. Res.*, 25 (1), 89-95, 1974.
- 782
- 783 Chau, J. H., C. Born, M. A. McGeoch, D. Bergstrom, J. Shaw, A. Terauds, M. Mairal, J. J. Le Roux and B. Jansen van Vuuren.  
784 The influence of landscape, climate and history on spatial genetic patterns in keystone plants (*Azorella*) on sub-Antarctic  
785 islands, *Mol. Ecol.*, 28 (14), 3291-3305, doi: <https://doi.org/10.1111/mec.15147>, 2019.
- 786
- 787 Deng, Y. N., S. J. Roberts, K. M. Saunders, B. Perren and C. Selfe. Late-Holocene palaeoecological reconstruction of Southern  
788 Hemisphere Westerlies variability on Subantarctic Macquarie Island, *The Holocene*, 09596836261432461, 2025.
- 789
- 790 Evans, A. J.: Some aspects of the ecology of a calenoid copepod, *Pseudoboekela brevicaudata*. Brady, 1875, on a subantarctic  
791 island, ANARE Scientific Reports, series B, 1, Zoology, 100, 1970.
- 792
- 793 Farqan, M., L. Xiang, J. Deng, H. Chen, W. Wang, S. Yu, Z. Zhu, C. Yan, C. Huang and X. Liu. Modern surface sediment  
794 diatom assemblages and conductivity modeling in northern China, *Ecol. Indicators*, 179, 114229, 2025.
- 795
- 796 Fitzgerald, N. B., J. B. Kirkpatrick and J. J. Scott. Rephotography, permanent plots and remote sensing data provide varying  
797 insights on vegetation change on subantarctic Macquarie Island, 1980–2015, *Austral Ecol.*, 46 (5), 762-775, 2021.
- 798

799 Fletcher, M.-S., J. Pedro, T. Hall, M. Mariani, J. A. Alexander, K. Beck, M. Blaauw, D. A. Hodgson, H. Heijnis and P. S.  
800 Gadd. Northward shift of the southern westerlies during the Antarctic Cold Reversal, *Quat. Sci. Rev.*, 271, 107189, 2021.  
801  
802 Fogt, R. L. and G. J. Marshall. The Southern Annular Mode: variability, trends, and climate impacts across the Southern  
803 Hemisphere, *Wiley Interdiscip. Rev. Clim. Change*, 11 (4), e652, 2020.  
804  
805 Gasse, F., P. Barker, P. A. Gell, S. C. Fritz and F. Chalieu. Diatom-inferred salinity in palaeolakes: an indirect tracer of climate  
806 change, *Quat. Sci. Rev.*, 16 (6), 547-563, 1997.  
807  
808 Gat, J. R.: Oxygen and hydrogen isotopes in the hydrologic cycle, *Annu. Rev. Earth Planet. Sci.*, 24 (1), 225-262, 1996.  
809  
810 Gillett, N. P., T. D. Kell and P. Jones. Regional climate impacts of the Southern Annular Mode, *Geophys. Res. Lett.*, 33 (23),  
811 2006.  
812  
813 Goeyers, C., D. H. Vitt and B. Van de Vijver. Taxonomic and biogeographical analysis of diatom assemblages from historic  
814 bryophyte samples from Campbell Island (sub-Antarctic), *Plant Ecol. Evol.*, 155 (1), 107-122, 2022.  
815  
816 Goldenberg Vilar, A., T. Donders, A. Cvetkoska and F. Wagner-Cremer. Seasonality modulates the predictive skills of diatom  
817 based salinity transfer functions, *PLOS ONE*, 13 (11), e0199343, doi: 10.1371/journal.pone.0199343, 2018.  
818  
819 Goyal, R., A. Sen Gupta, M. Jucker and M. H. England. Historical and projected changes in the Southern Hemisphere surface  
820 westerlies, *Geophys. Res. Lett.*, 48 (4), e2020GL090849, 2021.  
821  
822 Gremmen, N. J., B. Van De Vijver, Y. Frenot and M. Lebouvier. Distribution of moss-inhabiting diatoms along an altitudinal  
823 gradient at sub-Antarctic Îles Kerguelen, *Antarct. Sci.*, 19 (1), 17-24, 2007.  
824  
825 Humphries, R. S., M. D. Keywood, S. Gribben, I. M. McRobert, J. P. Ward, P. Selleck, S. Taylor, et al.: Southern Ocean  
826 latitudinal gradients of cloud condensation nuclei, *Atmos. Chem. Phys.*, 21 (16), 12757-12782, doi: 10.5194/acp-21-12757-  
827 2021, 2021.  
828  
829 Jones, J. M., S. T. Gille, H. Goosse, N. J. Abram, P. O. Canziani, D. J. Charman, K. R. Clem, et al.: Assessing recent trends in  
830 high-latitude Southern Hemisphere surface climate, *Nat. Clim. Change*, 6 (10), 917-926, doi: 10.1038/nclimate3103, 2016.  
831  
832 Juggins, S. C2 User Guide. Software for ecological and palaeoecological data analysis and visualisation. Newcastle-uponTyne,  
833 UK: University of Newcastle. 2003.  
834  
835 Juggins, S.: Quantitative reconstructions in palaeolimnology: new paradigm or sick science?, *Quat. Sci. Rev.*, 64, 20-32, 2013.  
836  
837 Keenan, H. M.: Modern and fossil terrestrial and freshwater habitats on subantarctic Macquarie Island, Macquarie University,  
838 Thesis, doi: <https://doi.org/10.25949/24796983.v1>, 1995.  
839  
840 Kennedy, B. and Y. M. Buckley. Use of seasonal epilithic diatom assemblages to evaluate ecological status in Irish lakes,  
841 *Ecol. Indicators*, 129, 107853, doi: <https://doi.org/10.1016/j.ecolind.2021.107853>, 2021.  
842  
843 Kong, Z., A. Prata, P. May, A. Purich, Y. Huang and S. Siems. Intensifying precipitation over the Southern Ocean challenges  
844 reanalysis-based climate estimates—Insights from Macquarie Island’s 45-year record, *EGU sphere*, 2025, 1-25, 2025.  
845  
846 Le Quéré, C., M. R. Raupach, J. G. Canadell, G. Marland, L. Bopp, P. Ciais, T. J. Conway, et al.: Trends in the sources and  
847 sinks of carbon dioxide, *Nat. Geosci.*, 2 (12), 831-836, doi: 10.1038/ngeo689, 2009.  
848

849 le Roux, P. C. and M. A. McGeoch. Rapid range expansion and community reorganization in response to warming, *Global*  
850 *Change Biol.*, 14 (12), 2950-2962, doi: <https://doi.org/10.1111/j.1365-2486.2008.01687.x>, 2008.  
851  
852 Lee, J. E. and S. L. Chown. Range expansion and increasing impact of the introduced wasp *Aphidius matricariae* Haliday on  
853 sub-Antarctic Marion Island, *Biol. Invasions*, 18 (5), 1235-1246, doi: 10.1007/s10530-015-0967-3, 2016.  
854  
855 Liao, M., U. Herzschuh, Y. Wang, X. Liu, J. Ni and K. Li. Lake diatom response to climate change and sedimentary events on  
856 the southeastern Tibetan Plateau during the last millennium, *Quat. Sci. Rev.*, 241, 106409, 2020.  
857  
858 Löffler, E.: Macquarie Island: A wind-molded natural landscape in the subantarctic, *Polar Geogr.*, 8 (4), 267-286, 1984.  
859  
860 Marchant, R., B. Kefford, J. Wasley, C. King, J. Doube and D. Nuggeoda. Response of stream invertebrate communities to  
861 vegetation damage from overgrazing by exotic rabbits on subantarctic Macquarie Island, *Mar. Freshw. Res.*, 62 (4), 404-413,  
862 2011.  
863  
864 Marshall, G. J.: Trends in the Southern Annular Mode from observations and reanalyses, *J. Clim.*, 16 (24), 4134-4143, 2003.  
865  
866 Maslennikova, A. V. e.: Development and application of an electrical conductivity transfer function, using diatoms from lakes  
867 in the Urals, Russia, *J. Paleolimnol.*, 63 (2), 129-146, 2020.  
868  
869 McBride, T.: Freshwater diatoms on sub-antarctic Macquarie Island: an ecological survey of 14 lakes, *Pap. Proc. R. Soc.*  
870 *Tasman.*, 143 (2), 2009.  
871  
872 McBride, T. P. and J. M. Selkirk. Palaeolake diatoms on sub-Antractic Macquarie Island: Possible markers of climate change,  
873 *Data Symposium 1998*.  
874  
875 Menviel, L. C., P. Spence, A. E. Kiss, M. A. Chamberlain, H. Hayashida, M. H. England and D. Waugh. Enhanced Southern  
876 Ocean CO<sub>2</sub> outgassing as a result of stronger and poleward shifted southern hemispheric westerlies, *Biogeosciences*, 20 (21),  
877 4413-4431, 2023.  
878  
879 Meredith, K., S. Hollins, C. Hughes, D. Cendón, S. Hankin and D. Stone. Temporal variation in stable isotopes (18O and 2H)  
880 and major ion concentrations within the Darling River between Bourke and Wilcannia due to variable flows, saline  
881 groundwater influx and evaporation, *J. Hydrol.*, 378 (3-4), 313-324, 2009.  
882  
883 Meredith, K. T., K. M. Saunders, L. K. McDonough and M. McGeoch. Hydrochemical and isotopic baselines for understanding  
884 hydrological processes across Macquarie Island, *Sci. Rep.*, 12 (1), 21266, doi: 10.1038/s41598-022-25115-3, 2022.  
885  
886 Molén, M. O.: Geochemical proxies: Paleoclimate or paleoenvironment?, *Geosyst. Geoenviron.*, 3 (1), 100238, 2024.  
887  
888 Mongwe, P., L. Gregor, J. Tjiputra, J. Hauck, T. Ito, C. Danek, M. Vichi, S. Thomalla and P. M. S. Monteiro. Projected  
889 poleward migration of the Southern Ocean CO<sub>2</sub> sink region under high emissions, *Commun. Earth Environ.*, 5 (1), 232, doi:  
890 10.1038/s43247-024-01382-y, 2024.  
891  
892 Nel, W., D. W. Hedding and E. M. Rudolph. The sub-Antarctic islands are increasingly warming in the 21st century, *Antarct.*  
893 *Sci.*, 35 (2), 124-126, 2023.  
894  
895 Nicholson, S.-A., D. B. Whitt, I. Fer, M. D. du Plessis, A. D. Lebéhot, S. Swart, A. J. Sutton and P. M. S. Monteiro. Storms  
896 drive outgassing of CO<sub>2</sub> in the subpolar Southern Ocean, *Nat. Commun.*, 13 (1), 158, doi: 10.1038/s41467-021-27780-w,  
897 2022.  
898

899 Oksanen, J., F. G. Blanchet, R. Kindt, P. Legendre, P. R. Minchin, R. O'hara, G. L. Simpson, P. Solymos, M. H. H. Stevens  
900 and H. Wagner. Package 'vegan', Community ecology package, version, 2 (9), 1-295, 2013.  
901  
902 Olivier, L. and F. A. Haumann. Southern Ocean freshening stalls deep ocean CO2 release in a changing climate, Nat. Clim.  
903 Change, 15 (11), 1219-1225, doi: 10.1038/s41558-025-02446-3, 2025.  
904  
905 Peng, Y., P. Rioual and Z. Jin. A record of Holocene climate changes in central Asia derived from diatom-inferred water-level  
906 variations in Lake Kalakuli (Eastern Pamirs, western China), Front. Earth Sci., 10, 825573, 2022.  
907  
908 Perren, B. B., D. A. Hodgson, S. J. Roberts, L. Sime, W. Van Nieuwenhuyze, E. Verleyen and W. Vyverman. Southward  
909 migration of the Southern Hemisphere westerly winds corresponds with warming climate over centennial timescales,  
910 Communications Earth and Environment, 1 (1), doi: 10.1038/s43247-020-00059-6, 2020.  
911  
912 Perren, B. B., J. Kaiser, H. W. Arz, O. Dellwig, D. A. Hodgson and F. Lamy. Poleward displacement of the Southern  
913 Hemisphere Westerlies in response to Early Holocene warming, Commun. Earth Environ., 6 (1), 164, doi: 10.1038/s43247-  
914 025-02129-z, 2025.  
915  
916 Recasens, C., D. Ariztegui, N. I. Maidana, B. Zolitschka and P. S. Team. Diatoms as indicators of hydrological and climatic  
917 changes in Laguna Potrok Aike (Patagonia) since the Late Pleistocene, Palaeogeogr., Palaeoclimatol., Palaeoecol., 417, 309-  
918 319, 2015.  
919  
920 Roberts, D., A. McMinn and D. Zwartz. An initial palaeosalinity history of Jaw Lake, Bunger Hills based on a diatom–salinity  
921 transfer function applied to sediment cores, Antarct. Sci., 12 (2), 172-176, 2000.  
922  
923 Sabbe, K., W. Vyverman, L. Ector, C. E. Wetzel, J. John, D. A. Hodgson, E. Verleyen and B. Van de Vijver. On the identity  
924 of *Navicula gottlandica* (Bacillariophyta), with the description of two new species *Navicula eileencoxiana* and *Navicula*  
925 *bergstromiana* from the Australo-Pacific region, Plant Ecol. Evol., 152 (2), 313-326, <https://www.jstor.org/stable/26672975>,  
926 2019.  
927  
928 Saunders, K. M., J. J. Harrison, D. A. Hodgson, R. de Jong, F. Mauchle and A. McMinn. Ecosystem impacts of feral rabbits  
929 on World Heritage sub-Antarctic Macquarie Island: A palaeoecological perspective, Anthropocene, 3, 1-8, doi:  
930 <https://doi.org/10.1016/j.ancene.2014.01.001>, 2013.  
931  
932 Saunders, K. M., D. A. Hodgson and A. McMinn. Quantitative relationships between benthic diatom assemblages and water  
933 chemistry in Macquarie Island lakes and their potential for reconstructing past environmental changes, Antarct. Sci., 21 (1),  
934 35-49, doi: 10.1017/S0954102008001442, 2009.  
935  
936 Saunders, K. M., D. A. Hodgson, S. McMurtrie and M. Grosjean. A diatom-conductivity transfer function for reconstructing  
937 past changes in the Southern Hemisphere westerly winds over the Southern Ocean, J. Quat. Sci., 30 (5), 464-477, doi:  
938 10.1002/jqs.2788, 2015.  
939  
940 Saunders, K. M., S. J. Roberts, B. Perren, C. Butz, L. Sime, S. Davies, W. Van Nieuwenhuyze, M. Grosjean and D. A. Hodgson.  
941 Holocene dynamics of the Southern Hemisphere westerly winds and possible links to CO2 outgassing, Nat. Geosci., 11 (9),  
942 650-655, doi: 10.1038/s41561-018-0186-5, 2018.  
943  
944 Scott, J. and J. Kirkpatrick. Rabbits, landslips and vegetation change on the coastal slopes of subantarctic Macquarie Island,  
945 1980–2007: implications for management, Polar Biol., 31 (4), 409-419, 2008.  
946  
947 Selkirk-Bell, J. and P. Selkirk. Vegetation-banked terraces on Subantarctic Macquarie Island: a reappraisal, Arct. Antarct. Alp.  
948 Res., 45 (2), 261-274, 2013.

949  
950 Selkirk, P., R. Seppelt and D. Selkirk. Subantarctic Macquarie Island: environment and biology, Cambridge University Press,  
951 1990.  
952  
953 Shaw, J., A. Terauds and D. Bergstrom. Rapid commencement of ecosystem recovery following aerial baiting on sub-Antarctic  
954 Macquarie Island, *Ecol. Manage. Restor.*, 12 (3), 241-244, 2011.  
955  
956 Springer, K.: Eradication of invasive species on Macquarie Island to restore the natural ecosystem, In: *Recovering Australian*  
957 *threatened species: A book of hope*, CSIRO Publishing, 13-22, 2018.  
958  
959 Sterken, M., E. Verleyen, V. Jones, D. Hodgson, W. Vyverman, K. Sabbe and B. Van de Vijver. An illustrated and annotated  
960 checklist of freshwater diatoms (Bacillariophyta) from Livingston, Signy and Beak Island (Maritime Antarctic Region), *Plant*  
961 *Ecol. Evol.*, 148 (3), 431-455, 2015.  
962  
963 Sterken, M., E. Verleyen, K. Sabbe, G. Terryn, F. Charlet, S. Bertrand, X. Boës, N. Fagel, M. De Batist and W. Vyverman.  
964 Late Quaternary climatic changes in southern Chile, as recorded in a diatom sequence of Lago Puyehue (40 40' S), *J.*  
965 *Paleolimnol.*, 39 (2), 219-235, 2008.  
966  
967 ter Braak, C. J. and S. Juggins. Weighted averaging partial least squares regression (WA-PLS): an improved method for  
968 reconstructing environmental variables from species assemblages, *Hydrobiologia*, 269 (1), 485-502, 1993.  
969  
970 Ter Braak, C. J. and I. C. Prentice. A theory of gradient analysis, In: *Advances in ecological research*, Elsevier, 271-317, 1988.  
971  
972 Terauds, A.: Changes in rabbit numbers on Macquarie Island 1974–2008, Report to Tasmanian Parks and Wildlife Service,  
973 2009.  
974  
975 Thomas, Z. A., H. Cadd, C. Turney, L. Becerra-Valdivia, H. A. Haines, C. Marjo, C. Fogwill, S. Carter and P. Brickle. Westerly  
976 wind shifts drove Southern Hemisphere mid-latitude peat growth since the last glacial, *Nat. Geosci.*, doi: 10.1038/s41561-025-  
977 01842-w, 2025.  
978  
979 Van de Vijver, B., Y. Freynot and L. Beyens. Freshwater diatoms from Ile de la Possession (Crozet archipelago, Subantarctica),  
980 *Bibliotheca Diatomologica*, 46, 1-412, 2002.  
981  
982 Van de Vijver, B.: *Aulacoseira principissa* sp. nov., a new 'centric' diatom species from the sub-Antarctic region, *Phytotaxa*,  
983 52, 33–42-33–42, 2012.  
984  
985 Van de Vijver, B.: Revision of the *Psammothidium manguinii* complex (Bacillariophyta) in the sub-Antarctic Region with the  
986 description of four new taxa, *Fottea*, 19 (1), 90-106, doi: 10.5507/fot.2019.001, 2019.  
987  
988 Van Nieuwenhuyze, W.: Diatom species and limnological data from 64 lakes on subantarctic Marion Island (2011) [Data set]:  
989 UK Polar Data Centre, Natural Environment Research Council, UK Research & Innovation, [https://doi.org/10.5285/1fa89ba7-](https://doi.org/10.5285/1fa89ba7-a904-43a8-a98d-ff887584221a)  
990 [a904-43a8-a98d-ff887584221a](https://doi.org/10.5285/1fa89ba7-a904-43a8-a98d-ff887584221a), 2020.  
991  
992 Verleyen, E., D. A. Hodgson, K. Sabbe, K. Vanhoutte and W. Vyverman. Coastal oceanographic conditions in the Prydz Bay  
993 region (East Antarctica) during the Holocene recorded in an isolation basin, *The Holocene*, 14 (2), 246-257, 2004.  
994  
995 Verleyen, E., D. A. Hodgson, W. Vyverman, D. Roberts, A. McMinn, K. Vanhoutte and K. Sabbe. Modelling diatom responses  
996 to climate induced fluctuations in the moisture balance in continental Antarctic lakes, *J. Paleolimnol.*, 30, 195-215, 2003.  
997

998 Volik, O., R. M. Petrone, R. I. Hall, M. L. Macrae, C. M. Wells, M. C. Elmes and J. S. Price. Long-term precipitation-driven  
999 salinity change in a saline, peat-forming wetland in the Athabasca Oil Sands Region, Canada: a diatom-based  
1000 paleolimnological study, *J. Paleolimnol.*, 58 (4), 533-550, 2017.  
1001  
1002